EFFECT OF DIFFERENT ANTIFER UNIT PLACEMENT METHODS ON WAVE OVERTOPPING

A THESIS SUBMITTED TO
THE GRADUATE SCHOOL OF NATURAL AND APPLIED SCIENCES
OF
MIDDLE EAST TECHNICAL UNIVERSITY

BY

BERKAY ERLER

IN PARTIAL FULFILLMENT OF THE REQUIREMENTS
FOR
THE DEGREE OF MASTER OF SCIENCE
IN
CIVIL ENGINEERING

SEPTEMBER 2023

Approval of the thesis:

EFFECT OF DIFFERENT ANTIFER UNIT PLACEMENT METHODS ON WAVE OVERTOPPING

submitted by **BERKAY ERLER** in partial fulfillment of the requirements for the degree of **Master of Science** i**n Civil Engineering, Middle East Technical University** by,

Prof. Dr. Halil Kalıpçılar
Dean, Graduate School of **Natural and Applied Sciences** _____

Prof. Dr. Erdem Canbay
Head of the Department, **Civil Engineering** _____

Prof. Dr. Ahmet Cevdet Yalçıner
Supervisor, **Civil Engineering, METU** _____

Dr. Hasan Gökhan Güler
Co-Supervisor, **Civil Engineering, METU** _____

Examining Committee Members:

Asst. Prof. Dr. Gülizar Özyurt Tarakcıoğlu
Civil Engineering, METU _____

Prof. Dr. Ahmet Cevdet Yalçıner
Civil Engineering, METU _____

Prof. Dr. Kubilay Cihan
Civil Engineering, Kırıkkale University _____

Asst. Prof. Dr. Cüneyt Baykal
Civil Engineering, METU _____

Asst. Prof. Dr. Doğan Kısacık
Civil Engineering, Izmir Institute of Technology _____

Date: 11.09.2023

I hereby declare that all information in this document has been obtained and presented in accordance with academic rules and ethical conduct. I also declare that, as required by these rules and conduct, I have fully cited and referenced all material and results that are not original to this work.

Name, Last name : Berkay Erler

Signature :

ABSTRACT

EFFECT OF DIFFERENT PLACEMENT METHODS OF ANTIFER UNITS ON WAVE OVERTOPPING

Erler, Berkay
Master of Science, Civil Engineering
Supervisor: Prof. Dr. Ahmet Cevdet Yalçıner
Co-Supervisor: Dr. Hasan Gökhan Güler

September 2023, 83 pages

Along with stability, the most important criterion in the design of rubble mound breakwaters is the serviceability, which is mostly determined based on wave overtopping. Wave overtopping discharges are generally estimated using available empirical formulas in the literature. The effect of different armor units on wave overtopping are reflected utilizing roughness coefficients (γ_f) in these empirical formulas in the widely accepted design specifications. However, the effect of different placement methods of these units are not completely addressed and discussed.

In this study, the effect of different placement methods of antifer units on wave overtopping were investigated. For this purpose, an experimental study was carried out at Middle East Technical University, Department of Civil Engineering, Coastal and Ocean Engineering Laboratory wave flume on a conventional rubble mound breakwater cross-section constructed using antifer units having a 1:2 face slope and crown walls with varying crest heights (R_c).The different antifer placement methods proposed in the literature, namely closed pyramid, double pyramid (regular and

staggered) and irregular placement methods were utilized, and experiments were carried out in a total of eight different armor layers by also considering different packing densities in each placement method. Wave steepnesses ($H_{m0}/L_{m-1,0}$) between 0.025 and 0.038 and relative crest freeboards (R_c/H_{m0}) between 0.68 and 1.85 were tested for each armor layer under five different irregular wave series.

Results of experimental studies show that different antifer unit placement methods and packing densities significantly change the wave overtopping discharges. It is observed that the mean wave overtopping rate obtained when antifer units are placed with the regular double pyramid placement method is 100% higher than the irregular placement method for the same packing density. Based on the experimental results, new roughness coefficients (γ_f) are proposed for different antifer unit placement methods.

Keywords: Antifer, Wave Overtopping, Roughness Coefficient, Individual Wave Overtopping

ÖZ

ANTİFER ÜNİTELERİNİN FARKLI DİZİLİMLERİNİN DALGA AŞMASINA ETKİSİ

Erler, Berkay
Yüksek Lisans, İnşaat Mühendisliği
Tez Yöneticisi: Prof. Dr. Ahmet Cevdet Yalçıner
Ortak Tez Yöneticisi: Dr. Hasan Gökhan Güler

Eylül 2023, 83 sayfa

Taş dolgu dalgakıranların tasarımında stabilitenin yanı sıra en önemli kriter işletilebilirliktir ve bu kriter çoğunlukla dalga aşmasına bağlı olarak belirlenir. Dalga aşma debileri genellikle literatürde mevcut ampirik formüller kullanılarak tahmin edilmektedir. Farklı koruma tabakası ünitelerinin dalga aşması üzerindeki etkisi, yaygın olarak kabul gören tasarım şartnamelerinde bu ampirik formüllerdeki pürüzlülük katsayıları (γ_f) kullanılarak yansıtılmaktadır. Ancak, bu ünitelerin farklı yerleştirme yöntemlerinin etkisi tam olarak ele alınmamış ve tartışılmamıştır.

Bu çalışmada, antifer ünitelerinin farklı yerleştirme yöntemlerinin dalga aşması üzerindeki etkisi araştırılmıştır. Bu amaçla, Orta Doğu Teknik Üniversitesi İnşaat Mühendisliği Bölümü Kıyı ve Deniz Mühendisliği Laboratuvarı dalga kanalında, 1:2 yüzey eğimine, farklı kret yüksekliklerine (R_c) ve kronman duvarla sahip, antifer üniteleri kullanılarak inşa edilen geleneksel bir taş dolgu dalgakıran kesiti üzerinde deneysel bir çalışma gerçekleştirilmiştir. Literatürde önerilen farklı antifer yerleştirme yöntemleri olan kapalı piramit, çift piramit ve düzensiz yerleştirme yöntemleri kullanılmış ve her bir yerleştirme yönteminde farklı yerleştirme sıklıkları da dikkate alınarak toplam sekiz farklı koruma tabakasında deneyler

gerçekleştirilmiştir. Dalga diklikleri ($H_{m0}/L_{m-1,0}$) 0.025 ile 0.038 arasında ve bağıl tepe yükseklikleri (R_c/H_{m0}) 0.68 ile 1.85 arasında değişen beş farklı düzensiz dalga serisi altında her bir koruma tabakası için test edilmiştir.

Deneysel çalışmaların sonuçları, farklı antifer ünitesi yerleştirme yöntemlerinin ve yerleştirme sıklıklerının dalga taşma deşarjlarını önemli ölçüde değiştirdiğini göstermektedir. Antifer üniteleri çift piramit yerleştirme yöntemi ile yerleştirildiğinde elde edilen ortalama dalga aşma oranının, aynı yerleştirme sıklığı için düzensiz yerleştirme yöntemine göre %100 daha yüksek olduğu görülmektedir. Deneysel sonuçlara dayanarak, farklı antifer ünitesi yerleştirme yöntemleri için yeni pürüzlülük katsayıları (γ_f) önerilmiştir.

Anahtar Kelimeler: Antifer, Dalga Aşması, Pürüzlülük Katsayısı, Tekil Dalga Aşması

To my family and friends

ACKNOWLEDGMENTS

I would like to express my deep thanks and gratitude to my advisor Prof. Dr. Ahmet Cevdet Yalçıner for his guidance through my both undergraduate and graduate education. He made the greatest contribution in my choice of coastal engineering by giving me this chance and supporting my interest in this field of engineering.

I would like to extend my sincere thanks to my co-supervisor Dr. Hasan Gökhan Güler for his support, guidance and dedication. He was always there whenever I had a problem, whether it was academic related or not.

I would also like to thank Asst. Prof. Dr. Cüneyt Baykal, who trusted me with the project in the laboratory which turned out to be this thesis. He virtually is the third advisor of this research whom I had great pleasure to work with.

I would like to express my special thanks Prof. Dr. Ayşen Ergin, who introduced me to coastal engineering during my undergraduate years and paved the way for more. I am grateful for her always high energy, loving support and help that fueled my enthusiasm.

I would like to extend my sincere thanks to Dr. Işıkhan Güler for his engineering perspective and profound experience that he shared with us. Both working as an intern with him and being a student of his was an educational experience.

I would like to thank Asst. Prof. Dr. Gülizar Özyurt Tarakcıoğlu for her collaboration with us on the project. Her constructive feedback was a great help and an essential part of this study that I will remember.

I would like to thank Yusuf Korkut, Servet Şeherli and Eyüp Uğur, who have helped however they can in order to solve problems that occurred about our experiment

setup. They always offered their support without hesitation. This thesis study could not have been completed without their valuable help.

I would like to thank all my friends in Coastal and Ocean Engineering Laboratory who walked the same path and faced the same hardships. It was a pleasure to study and work with them.

I would like to express my special thanks to my brothers, Furkan Demir, Cem Sevindik, Mert Yaman, Barış Ufuk Şentürk and Günay Gazaloğlu, for sharing long days in the lab. Their help and support along the way has been invaluable.

I would like to express my deepest thanks to the people of Mizantrop where I spend the most time outside the laboratory. I am deeply grateful to Oya and Emre Kuzum for creating a place for strangers from distant lands and friends of old to gather.

I would like to extend my deepest thanks to my friends: Sinem Asar, Murat Ural, Samet Albayrak, Ceyda Yolgörmez, Bekir Doğru, Canan Ece Türkmen and Melike Başak Yalçın who are always there through good and bad. They make life brighter for me.

Lastly, I would like to express my deepest gratitude to my family: my mother Ayşe Gül Erler, my father Serdar Erler, my sister Simden Erler, and my aunt Asuman Yürükoğlu. I am thankful for their unconditional and endless love and support.

This work is totally funded by the Scientific and Technological Research Council of Turkey under grant number TUBİTAK 122M053. We acknowledge the financial support from TUBITAK.

TABLE OF CONTENTS

ABSTRACT v
ÖZ vii
ACKNOWLEDGMENTS x
TABLE OF CONTENTS xii
LIST OF TABLES xv
LIST OF FIGURES xvii
LIST OF ABBREVIATIONS xx
LIST OF SYMBOLS xxi
1 INTRODUCTION 1
2 LITERATURE REVIEW 5
2.1 Breakwater Section Design 5
2.1.1 Armor Unit Placement Methods 6
2.2 Wave Overtopping Measurement 8
2.3 Mean Wave Overtopping Prediction 10
2.3.1 Effect of Armor Layer Roughness 12
2.3.2 EurOtop (2018) 13
2.4 Individual Wave Overtopping Prediction 14
2.4.1 EurOtop (2018) 15
2.4.2 Molines et. al (2019) 17
2.4.3 Mares-Nasarre et al. (2020 18
3 METHODOLOGY 21
3.1 Experimental Setup 21

3.2 Wave Characteristics....23
3.3 Breakwater Section Design....24
3.4 Antifer Placement Methods....26
3.4.1 Closed Pyramid Placement....26
3.4.2 Regular Double Pyramid and Staggered Double Pyramid Placements....27
3.4.3 Irregular Placement....27
3.5 Wave Measurements....30
3.6 Overtopping Measurements....31
3.7 Test Conditions....37
3.8 Analysis Methods....38
3.8.1 Error Analysis....38
3.8.2 Determination of Roughness Coefficient....39
3.8.3 Mean Wave Overtopping Discharge Analysis....39
3.8.4 Individual Wave Overtopping Analysis....40
4 RESULTS....41
4.1 Roughness Coefficients....41
4.2 Mean Wave Overtopping....46
4.2.1 Effect of Placement Method....47
4.2.2 Effect of Packing Density....48
4.2.3 Evaluation of the Effect of New Roughness Coefficients on Mean Wave Overtopping Prediction Methods....52
4.3 Individual Wave Overtopping....61
4.3.1 Efefct of Placement Method....61

4.3.2 Evaluation of Individual Wave Overtopping Volume Prediction Methods 62

5 CONCLUSION 77

REFERENCES 81

LIST OF TABLES

TABLES

Table 2.1 Roughness coefficents, Bruce et al. (2009) 13
Table 2.2 Roughness coefficients, EurOtop (2018) 14
Table 2.3 Summary of the studies on individual wave overtopping 15
Table 3.1 Irregular wave series parameters 23
Table 3.2 Breakwater section dimensions 25
Table 3.3 Relative crest elevations 25
Table 3.4 Antifer unit placements 26
Table 3.5 Antifer unit placements and properties 28
Table 4.1 Error analysis results for γ_f and $\gamma_{f,n}$ 41
Table 4.2 Error analysis results for mean overtopping discharge prediction methods for DP_{reg} placement method 53
Table 4.3 Error analysis results for mean overtopping discharge prediction methods for DP_{stag} placement method 54
Table 4.4 Error analysis results for mean overtopping discharge prediction methods for CP placement method 56
Table 4.5 Error analysis results for mean overtopping discharge prediction methods for IR placement method 57
Table 4.6 Error analysis results for mean overtopping discharge prediction methods 59
Table 4.7 Error analysis results for maximum individual overtopping volume prediction methods for DP_{reg} placement method 63
Table 4.8 Error analysis results for maximum individual overtopping volume prediction methods for DP_{stag} placement method 65
Table 4.9 Error analysis results for maximum individual overtopping volume prediction methods for CP placement method 67

Table 4.10 Error analysis results for maximum individual overtopping volume prediction methods for IR placement method 69
Table 4.11 Error analysis results for maximum individual overtopping volume prediction methods 72

LIST OF FIGURES

FIGURES

Figure 2.1 Armor placement methods, Frens (2007) 7
Figure 2.2 Overtopping discharge collection system, Pillai et al. (2017) 8
Figure 2.3 Weight cell method scheme, Victor and Troch (2010) 9
Figure 2.4 Overtopping detection and measurement setup, Koosheh et al. (2022) .. 9
Figure 3.1 Wave flume 22
Figure 3.2 Camera views from front (a) and side (b) 22
Figure 3.3 Breakwater section 25
Figure 3.4 Overtopping detection system 31
Figure 3.5 Overtopping gutter 32
Figure 3.6 Overtopping tank 33
Figure 3.7 Overtopping collection tank 33
Figure 3.8 Overtopping event detected by cameras 34
Figure 3.9 Water level change for WG13 and WG14 36
Figure 3.10 Individual wave overtopping analysis for CP2 placement method under W3 wave condition 37
Figure 4.1 Distribution of mean wave overtopping discharges for all placement methods 42
Figure 4.2 Distribution of mean wave overtopping discharges for DP_{reg} placement method 43
Figure 4.3 Distribution of mean wave overtopping discharges for DP_{stag} placement method 44
Figure 4.4 Distribution of mean wave overtopping discharges for CP placement method 45
Figure 4.5 Distribution of mean wave overtopping discharges for IR placement method 46
Figure 4.6 Distribution of mean wave overtopping discharges for DP_{reg} and DP_{stag} placement methods 48

Figure 4.7 Distribution of mean wave overtopping of DP_{reg} placement method for two packing densities 49
Figure 4.8 Distribution of mean wave overtopping of DP_{stag} placement method for two packing densities 49
Figure 4.9 Distribution of mean wave overtopping of CP placement method for two packing densities 50
Figure 4.10 Distribution of mean wave overtopping of IR placement method for two packing densities 51
Figure 4.11 Comparison of measured and calculated mean wave overtopping discharges for DP_{reg} placement method 52
Figure 4.12 Comparison of measured and calculated mean wave overtopping discharges for DP_{stag} placement method 54
Figure 4.13 Comparison of measured and calculated mean wave overtopping discharges for CP placement method 55
Figure 4.14 Comparison of measured and calculated mean wave overtopping discharges for IR placement method 57
Figure 4.15 Comparison of measured and calculated (with $\gamma_f = 0.50$) mean wave overtopping discharges 58
Figure 4.16 Comparison of measured and calculated (with $\gamma_{f,n}$) mean wave overtopping discharges 59
Figure 4.17 Distribution of maximum individual wave overtopping volumes for all placement methods 61
Figure 4.18 Comparison of measured and calculated maximum individual overtopping volumes for DP_{reg} placement method (q_{calc} is predicted with $\gamma_f = 0.50$) 63
Figure 4.19 Comparison of measured and calculated maximum individual overtopping volumes for DP_{reg} placement method (q_{calc} is predicted with γ_{fn}) 64
Figure 4.20 Comparison of measured and calculated maximum individual overtopping volumes for DP_{stag} placement method (q_{calc} is predicted with $\gamma_f = 0.50$) 65

Figure 4.21 Comparison of measured and calculated maximum individual overtopping volumes for DP_{stag} placement method (q_{calc} is predicted with $\gamma_{f,n}$) 66
Figure 4.22 Comparison of measured and calculated maximum individual overtopping volumes for CP placement method (q_{calc} is predicted with $\gamma_f = 0.50$) . 67
Figure 4.23 Comparison of measured and calculated maximum individual overtopping volumes for CP placement method (q_{calc} is predicted with $\gamma_{f,n}$) 68
Figure 4.24 Comparison of measured and calculated maximum individual overtopping volumes for IR placement method (q_{calc} is predicted with $\gamma_f = 0.50$) .. 70
Figure 4.25 Comparison of measured and calculated maximum individual overtopping volumes for IR placement method 70
Figure 4.26 Comparison of measured and calculated maximum individual overtopping volumes where q_{calc} is predicted with $\gamma_f = 0.50$ 72
Figure 4.27 Comparison of measured and calculated maximum individual overtopping volumes where q_{calc} is predicted with $\gamma_{f,n}$ 73
Figure 4.28 Comparison of measured and calculated maximum individual overtopping volumes where q_{meas} is used as prediction 73

LIST OF ABBREVIATIONS

2D	Two dimensional
ANN	Artificial neural network
AYGM	Altyapı Yatırımları Genel Müdürlüğü
CI	Confidence interval
CP	Closed pyramid placement method
DP	Double pyramid placement method
DP_{reg}	Regular double pyramid placement method
DP_{stag}	Staggered double pyramid placement method
CLASH	Crest Level Assessment of Coastal Structures By Full Scale Monitoring, Neural Network Prediction and Hazard Analysis on Permissible Wave Overtopping
IR	Irregular placement method
MALE	Mean absolute logarithmic error
METU	Middle East Technical University
NN	Neural network
RMSLE	Root mean square logarithmic error
SPM	Shore Protection Manual
TAW	Technical Advisory Comitee on Flood Defence
WG	Wave gauge

LIST OF SYMBOLS

α	Angle of breakwater armour slope
Γ	Mathematical gamma function
γ	Peak enhancement factor for the JONSWAP spectrum
γ_β	Obliquity factor
γ_b	Berm factor
γ_f	Roughness factor
$\xi_{m-1,0}$	Surf similarity parameter corresponding to spectral mean wave period
ρ_s	Density of solid
ρ_w	Density of water
A	Scale factor
A_c	Armour crest freeboard of structure
b	Shape factor
c_d	Maximum wave celerity defined by L_{0p}/T_p
d_w	Distance between the two wave gauges
D_{n50}	Nominal diameter of the breakwater units
g	Gravitational acceleration
h	Water depth
H	Wave height
$H_{1/10}$	Significant wave height
H_{m0}	Spectral significant wave height

H_s	Significant wave height
K_D	Stability coefficient
L_0	Deep water wavelength
L_{0p}	Deep water wavelength corresponding to peak wave period
M_{50}	Median weight of the armour units in tons
N	Number of waves
N_{ov}	Number of overtopping events
O_n	Observed values
P_n	Predicted values
P_{ov}	Exceedance probability of an individual wave overtopping event
q	Mean wave overtopping discharge
q^*	Non-dimensional mean wave overtopping discharge
Q^*	Non-dimensional mean wave overtopping discharge
q_{mean}	Mean wave overtopping discharge
R_c	Crest freeboard of structure
R_c/H_{mo}	Relative crest freeboard of structure
R_u	Wave run-up level
$R_{u2\%}$	Wave run-up level exceeded by 2% of incident waves
$s_{m-1,0}$	Local wave steepness corresponding to spectral mean wave period
S_f	Sampling rate
s_{op}	Deep water wave steepness corresponding to peak wave period

T_{01}	Mean wave period defined by m_0/m_1
T_m	Mean wave period from time-domain analysis
$T_{m-1,0}$	Spectral mean wave period defined by m_{-1}/m_0
T_s	Significant wave period
T_p	Spectral peak wave period
$\overline{V}$	Mean of individual wave overtopping volumes
V_{max}	Maximum individual wave overtopping volume
V_{max}^*	Non- dimensional maximum individual wave overtopping volume

CHAPTER 1

INTRODUCTION

Coastal regions, with their beauty, and ecological and economical significance, have long been favored for human habitation and development. However, they are constantly exposed to natural forces where land, water and air interact. The objective of coastal engineering is understanding such forces and complex interactions and their impacts in order to guard coastal communities, structures and the ecosystem.

For safer and effective usage of coastal regions, areas that are protected from wave actions should be provided, such as harbors and ports that generally have defense structures as breakwaters. There are several construction methods of breakwaters including rubble mound, piled, vertical wall or floating depending on the area's needs, geomorphology, and wave climate.

Overtopping is the process where waves surpass the crest of a breakwater, leading to the potential discharge of significant volumes of water into the protected side. Estimating the wave overtopping is an essential part of breakwater design to ensure the overall effectiveness and safety of the structure that depends on wave climate, structure geometry water level and roughness of the breakwater surface. Researchers and engineers utilize various tools, including numerical models like ANN (Artificial Neural Networks), to predict wave overtopping rates based on these parameters. Additionally, empirical formulas such as the EurOtop (2018) formula are commonly used in practice to estimate wave overtopping and guide the design of rubble mound breakwaters. These tools and formulas contribute to the optimization and reliable

design of rubble mound breakwaters, ensuring coastal resilience and safeguarding against wave-induced damage.

The roughness characteristics of the surface in rubble mound breakwaters are mainly determined by the type and size of the armor layer units in the empirical formulas and artificial neural network tools used to compute the wave overtopping discharges. The effect of roughness along the armor layers of rubble mound breakwaters is investigated by experimental studies (e.g. Bruce et al., 2009). However, the effect of different placement of armor units on wave overtopping has not been studied.

In this study, physical model experiments are conducted for investigating the effects of different placement of antifer units on wave overtopping for a conventional rubble mound breakwater at the Middle East Technical University Civil Engineering Coastal and Ocean Engineering Laborator.

The research question focuses on investigating how different placement methods of antifer units impact the wave overtopping. It suggests that the study will explore the relationship between placement techniques and wave overtopping outcomes in coastal structures.

Main questions to be researched are:

i. What is the effect of different placement methods of antifer units on both mean and individual wave overtopping?
ii. How does the roughness coefficient change with different placement methods of antifer units?

To try to answer the abovementioned research questions, the present study is structured as follow:

In Chapter 2, a literature review is given for background information on the subject.

In Chapter 3, methodology for the experiments and analysis of the results are given. Within the scope of the study, A rubble mound breakwater section in a wave channel with no foreshore slope was constructed using antifer units in the armor layer. The

different antifer placement methods proposed by Frens (2007), namely closed pyramid, double pyramid (regular and staggered), and irregular unit placement methods were used with two different packing densities for each placement method to observe the effect of packing density as well. Irregular wave series with varying wave steepness and relative crest heights were selected and calibrated in the wave flume. All wave conditions are applied for each placement method in the experiments and conditions that may commonly occur in practical applications were studied. In the design of the breakwater using antifer units, the unit weights were chosen to be relatively high, thus preventing damage to the breakwater section. Design, measurement and analysis procedures for wave overtopping experiments in detail are given in this chapter.

In Chapter 4, results are presented and discussed for mean and indiviual wave overtopping measurements. Corresponding roughness coefficients are derived utilizing the mean overtopping measurements. On the other hand, the performances of the approaches to determine the maximum overtopping volumes are evaluated based on the individual wave overtopping measurements.

In Chapter 5, conclusions and future recommendations are given.

CHAPTER 2

LITERATURE REVIEW

The main objective of this study is to investigate the effect of different units used in the armor layer of rubble mound breakwaters and their placement on wave overtopping through experimental studies. For this purpose, wave series generation, wave measurement, overtopping measurement and breakwater cross section design methods for experimental studies and analysis methods are researched in the literature.

2.1 Breakwater Section Design

In a wave flume, one of the most challenging problems when generating waves is to isolate the reflected waves, as waves are reflecting from any solid boundaries inside the flume. Mansard and Funke (1980) propose a method that utilizes three wave gauges to isolate the incident and reflected wave spectra to examine a series of irregular waves. Goda and Suzuki (1976) also propose a method that separates the incident and reflected waves from the records of composite waves thatutilizes two wave gauge positions. Thus, one can make sure that the generated wave properties are in agreement with the target wave characteristics. The guidelines of Klopman and van der Meer's (1999) provide the distances between wave gauges in front of the structure, which can be applied together with Mansard and Funke (1980) method. These standard procedures are important to be considered when designing and testing breakwater cross-sections. For the cross-section design, AYGM's (2016) criteria for a conventional single slope rubble mound breakwater design gives a detailed method that is widely used in coastal structure construction in Turkey. For

the armor layer, the Hudson (SPM, 1984) approach (see Equation (2.1)), which relies on depth-induced wave breaking, can be used to determine the dimensions of the armor units (e.g. antifer units).

$$M_{50} = \frac{\rho_s H^3}{K_D \left(\frac{\rho_s}{\rho_w} - 1\right)^3 cot\alpha} \tag{2.1}$$

In this formula, ρ_s and ρ_w represent the mass density of the armor unit and water, respectively. H stands for the characteristic wave height (either H_s or $H_{1/10)}$, and D_{n50} represents the equivalent cube length of the armor unit. K_D is the stability coefficient, and α denotes the slope angle.

The determination of the crest elevation of the breakwater depending on the wave overtopping values is made by means of empirical formulas available in the literature (Manual on wave overtopping of sea defenses and related structures (EurOtop), 2018). For core layer rock mass calculations, Burcharth et al. (1999) considers viscosity induced effects for scaling. For the design of the crown wall, on the other hand, the approach given by Pedersen (1996) is widely used.

2.1.1 Armor Unit Placement Methods

Since this study focuses on only antifer units for the armor layer units, literature review covers researches on antifer units only. Yagci and Kapdasli (2003) and Yagci et al. (2004) investigated stability of alternative placement method and irregular placement respectively. Soltanpour and Yazdani (2009) conducted experiments in order to investigate the impact of diagonal regular and irregular antifer placement methods on wave run-up. There are also several conference papers on armor layer stability for different placement methods with limited conditions. However, the most extensive and relatively new study that gives detailed explanations on different armor unit placement methods to be found is the thesis research of Frens (2007).

Frens (2007) gives recommendations on the optimal placement of antifer units for cross-sectional stability. In his research, he conducted 17 experiments on a rubble mound structure with different antifer unit placement methods and packing densities. The tested methods, namely, closed pyramid, regular pyramid (regular and staggered), irregular placement methods are given in Figure 2.1.

According to this research's results, regular placement methods showed greater stability compared to irregular placement methods, even when they had a similar packing density. Furthermore, the increased irregularity of blocks within a regular placement method led to reduced stability. Placement methods with higher packing densities also exhibited greater stability and higher reflection coefficients. The resulting K_D values were within the range of 4.0 to 23.7. High reflection coefficients during the initial wave series resulted in longer berm lengths, indicating a positive correlation between reflection and overtopping.

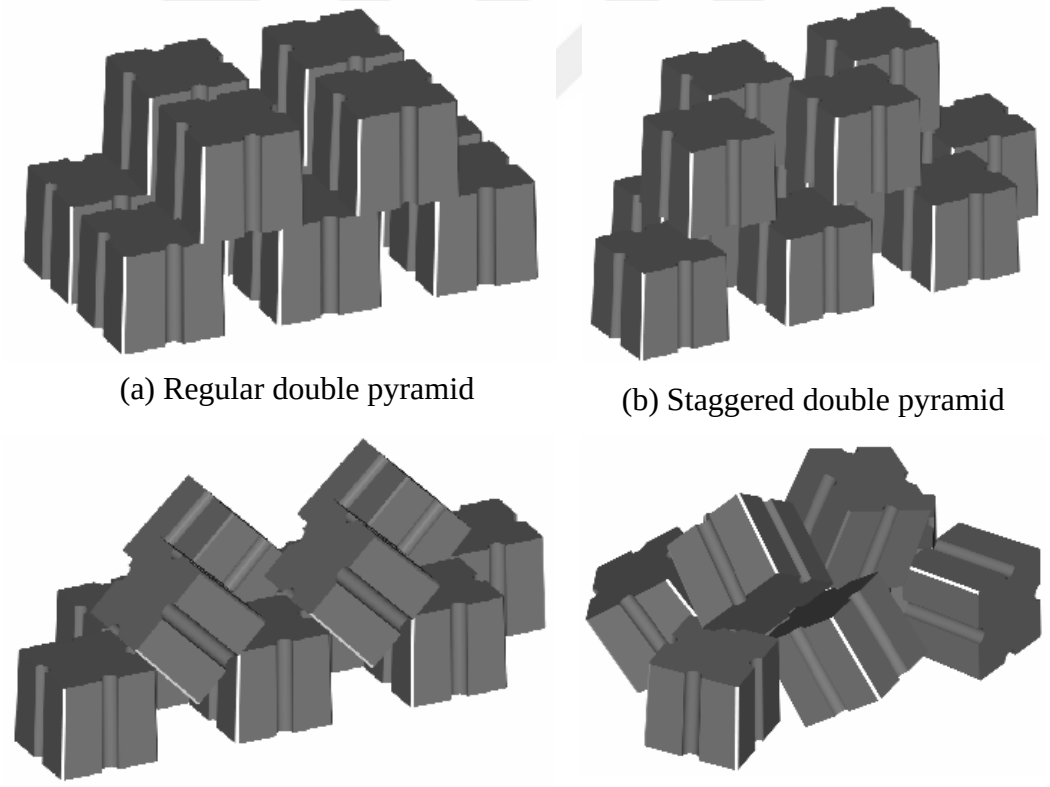

(a) Regular double pyramid

(b) Staggered double pyramid

(c) Closed pyramid

(d) Irregular

Figure 2.1 Armor placement methods, Frens (2007)

In summary, when the under layer and the toe are smooth, and block placement is precise, the most effective placement methods are the closed pyramid placement method (see Figure 2.1 (c)) for packing densities around 45% and 50%, and the regular double pyramid placement method (see Figure 2.1 (a)) for packing densities around 55% and 60%. Additionally, for double pyramid placement, when the second layer was shifted by half a nominal diameter, the reflection coefficients were minimized.

2.2 Wave Overtopping Measurement

For mean wave overtopping discharge measurements in literature, the accepted method is quite simple, as it is to place a overtopping unit that collects the total volume behind the structure, then measure the total volume. Schoonees et al. (2021) uses this method on their full-scale experiments for investigating mean wave overtopping at stepped revetments. Pillai et al. (2017) also follows this method on small-scale experiments for investigating a new mean wave overtopping discharge prediction formula for berm breakwaters (see Figure 2.2).

Figure 2.2 Overtopping discharge collection system, Pillai et al. (2017)

On the other hand, measuring individual wave overtopping volumes have been a challenge. There are several methods proposed in the literature that requries constant recording of overtopping volume collected and detect separate events in postprocessing of the data. Victor and Troch (2010) proposedan individual wave

overtopping detection and measurement system that utilizes a weight cell placed under the overtopping collection box recording the weight changes over time (see Figure 2.3).

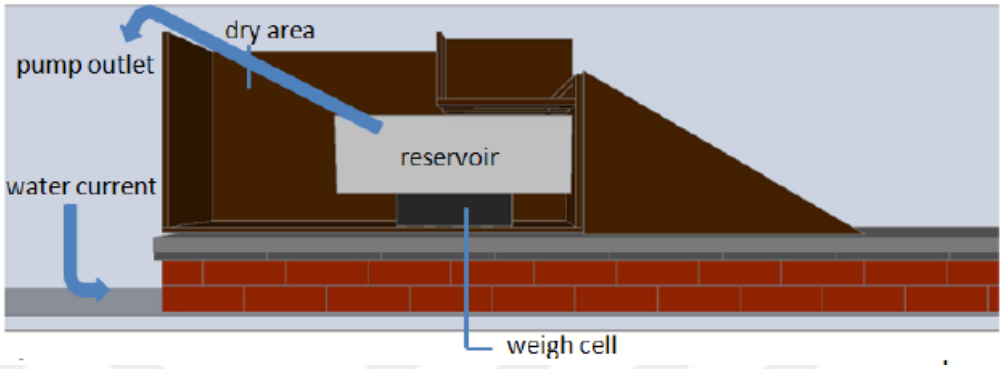

Figure 2.3 Weight cell method scheme, Victor and Troch (2010)

Besides weight cell measurements, there are also methods that utilize wave gauges by recording the water level in thecollection box. The most recent research that utilizes this method was conducted by Koosheh et al. (2022). In their study, Koosheh et al. (2022) investigated the distribution of individual overtopping volumes at seawalls. They conducted two dimensional (2D) physical experiments in a wave flume using a setup that detects and measures overtopping waves and their volumes (see Figure 2.4).

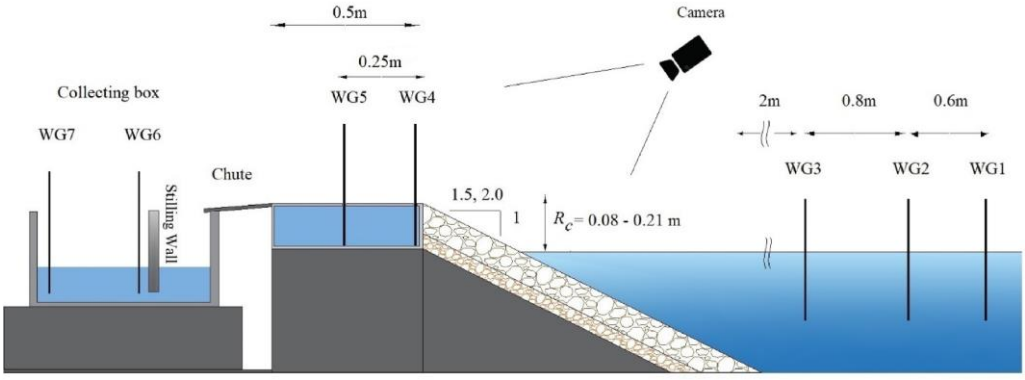

Figure 2.4 Overtopping detection and measurement setup, Koosheh et al. (2022)

In this setup, they place a chute that collects the overtopped water into a box that is placed behind the structure. This chute is placed at the center of the flume to prevent

boundary layer effects may be caused by flume walls. Individual overtopping volume measurements were conducted by recording the water surface level inside the box. To achieve this, two wave gauges (WG6 and WG7) with an initial submergence depth of 100 mm were placed at opposite corners of the box, and their average records were used to calculate overtopping volumes. To minimize water surface fluctuations resulting from falling water, particularly during large events, a stilling wall was placed within the container. Determining the number of overtopping waves (N_{ov}) based solely on the wave gauge records inside the container proved challenging due to small overtopping events that may go unnoticed when they occur immediately before or after a significant overtopping event. Therefore, two additional wave gauges (WG4 and WG5) were placed on the seaward edge and the midpoint of the crest to detect overtopping events. The data collected from the wave gauges were captured using a National Instruments data acquisition card and a self-developed MATLAB script, with a sampling frequency of 20 Hz. Additionally, two high-speed cameras were positioned above and beside the tank to complement and ensure the quality of the wave gauge data during the post-processing stage.

During the experiments, there were no notable variations in the paths of the overtopping waves, and the presence of wave gauges did not impact the overtopping flow on the smooth crest. The highest variation observed was 0.5% between the overall volume collected in the container and the sum of individual overtopping volumes in a single test. This finding confirms that very minor overtopping volumes were measured with a satisfactory level of accuracy with this method.

2.3 Mean Wave Overtopping Prediction

Along with stability, the most important design criterion in the design of rubble mound breakwaters is the determination of the serviceability of the breakwater. The serviceability of breakwaters is mostly determined based on wave overtopping. In the literature, the effect of unit types (e.g., quarry stone, antifer, tetrapod, etc.) on wave run-up and wave overtopping is calculated with the roughness coefficient

depending on the armor layer unit type (Bruce et al. 2009; EurOtop, 2018). These formulas are usually expressed in the form of Equation (2.2). It is a Weibull-shaped function with the dimensionless overtopping discharge $q/(gH_{mo}^3)^{1/2}$ and the relative crest freeboard R_c/H_{m0}.

$$\frac{q}{\sqrt{g \cdot H_{m0}^3}} = a \cdot exp\left[-\left(b \frac{R_c}{H_{m0} \cdot \gamma_f \cdot \gamma_\beta}\right)^c\right] \text{ for } R_c \geq 0 \tag{2.2}$$

In Equation (2.2), H_{mo} is mean wave height and R_c is crest elevation in meters. γ_f is roughness coefficient that depends on the unit types used in the armor layer of the structure and γ_β is the influence factor for oblique wave attack for mean wave overtopping calculations. Coefficients a, b and c change according to the structure type such as coastal dikes, embankment seawalls, armored rubble mounds and slopes, and vertical and steep walls.

There are also artificial neural networks such as CLASH ANN (or CLASH NN) provided by Deltares and EurOtop ANN provided by EurOtop, that predict overtopping rates based on structure dimensions and wave characteristics. The main distinction between the two artificial neural networks is that the CLASH NN is unable to forecast extremely minor overtopping flow rates and it has been built on smaller number of tests compared to EurOtop ANN. However, the effect of different arrangement methods of the units on wave overtopping is not addressed in these methods.

Moreover, as mentioned, Frens (2007) gives detailed information on stability of different antifer placement methods on the armor layer, and shares observations based on experimental tests on the relationship between wave overtopping, packing density and reflection. According to Frens (2007), there is a positive correlation between wave overtopping and wave reflection. Moreover, increasing the packing density results in a more stable armor layer, however, it yields higher reflection, thus, higher overtopping.

2.3.1 Effect of Armor Layer Roughness

One of the most prominent studies that investigated the roughness for different armor layerunits is done by Bruce et al. (2009). In this study outlines a large number of small-scale 2D physical model experiments aimed at enhancing the understanding of how the type of armor layer units affect overtopping. 179 tests are conducted to assess the relative impact of 13 different armor types and configurations on overtopping behavior. These tests included the determination of roughness coefficients (γ_f) for various materials, such as rock (in two layers), cubes (single layer and double layer), Tetrapod, Antifer, Haro, Accropode, Core-Loc™, and Xbloc™. These roughness influence factors have been integrated into the CLASH database and are intended for use in neural network predictions of overtopping.

In this study overtopping predictions are done according to Equation (2.3) proposed by TAW (2002). For antifer unit experiments, relative crest freeboards R_c/H_{m0} were 1.3 and 0.8, with R_c=128.7 mm and 79 mm.

$$\frac{q}{\sqrt{g \cdot H_{m0}^3}} = 0.2 \cdot exp\left(-2.6 \frac{R_c}{H_{m0} \cdot \gamma_f \cdot \gamma_\beta}\right) \tag{2.3}$$

Roughness coefficient results of this study for given armor layer unit types are given in Table 2.1. Values were normalized by comparing them to smooth slope tests with γ_f=1 as a reference point. Along with the average γ_f value, values at the lower and upper bounds of the 95% confidence interval (CI) are also provided in this study. Rock armor values, indicated in italics, were sourced from Van der Meer (1988).

Table 2.1 Roughness coefficents, Bruce et al. (2009)

Type of armor layer	**No. of layers**	γ_f **(mean)**	γ_f **(95% CI, low)**	γ_f **(95% CI, high)**
Smooth impermeable surface	-	1.00		
Rocks (impermeable core)	1	*0.60*		
Rocks (permeable core)	1	*0.45*		
Rocks (impermeable core)	2	*0.55*		
Rocks (permeable core)	2	0.40	0.37	0.43
Cubes	1	0.49	0.46	0.55
Cubes	2	0.47	0.44	0.50
Antifers	2	0.50	0.46	0.55
HARO's	2	0.47	0.44	0.50
Tetrapods	2	0.38	0.35	0.42
Accropode	1	0.46	0.43	0.48
Xbloc	1	0.44	0.41	0.49
Core-Loc	1	0.44	0.41	0.47
Dolosse	2	0.43		
Berm breakwater	2	0.40		
Icelandic berm breakwater	2	0.35		

2.3.2 EurOtop (2018)

For wave overtopping predictions, the most well-known methodology is the one proposed by EurOtop (2018) (Equation (2.4)) that considers wave characteristics, the type of units used in the armor layer, and the height of the crown wall.

$$\frac{q}{\sqrt{g \cdot H_{m0}^3}} = 0.09 \cdot exp\left[-\left(1.5 \frac{R_c}{H_{m0} \cdot \gamma_f \cdot \gamma_\beta}\right)^{1.3}\right] \tag{2.4}$$

Equation (2.4) considers rubble mound structures with slopes 1:2 to 1:4/3. EurOtop's (2018) suggestion for γ_f values are given in Table 2.2. While most of these values are based on both Bruce et al. (2009), values in italics are estimated or extrapolated according to CLASH results and modified according to Bruce et al. (2009). As a

result, EurOtop (2018) recommends γ_f = 0.50 for armor layers consisting of antifer units without making a distinction between placement methods.

Table 2.2 Roughness coefficients, EurOtop (2018)

Type of armor layer	γ_f
Smooth impermeable surface	1.00
Rocks (1 layer, impermeable core)	0.60
Rocks (1 layer, permeable core)	0.45
Rocks (2 layers, impermeable core)	0.55
Rocks (2 layers, permeable core)	0.40
Cubes (1 layer, flat positioning)	0.49
Cubes (2 layers, random positioning)	0.47
Antifers	0.50
HARO's	0.47
Tetrapods	0.38
Dolosse	*0.43*
Accropode I	0.46
Xbloc, Core-Loc, Accropode II	0.44
Cubipods (1 layer)	*0.49*
Cubipods (2 layers)	*0.47*

2.4 Individual Wave Overtopping Prediction

Mean wave overtopping flows, represented are frequently used for establishing the crest height of coastal structures. Nonetheless, the average volume of individual overtopping instances might significantly differ from the highest volume of an individual wave overtopping event, Franco et al. (1994) to propose a direct correlation between overtopping risk and individual wave overtopping occurrences, as opposed to relying only on the mean overtopping rate.

For prediction of maximum individual wave overtopping volume (V_{max}), there are various recent studies available in the literature that consider different structure types and relative crest freeboard ranges. A summary of these studies is given in Table 2.3. There are two important parameters that separates these methods for estimating V_{max},

namely the mean overtopping discharge (q) prediction and the exceedance probability of an individual wave overtopping event (P_{ov}) that depends on Weibull parameters such as shape and scale factors.

Table 2.3 Summary of the studies on individual wave overtopping

Reference study	Structure type	R_c/H_{m0}
Victor et al. (2012)	Steep slopes - Smooth - Impermeable	$0.1 \leq R_c/H_{m0} \leq 1.69$
Nørgaard et al. (2014)	Sea dike - Rough - Permeable	$0.9 \leq R_c/H_{m0} \leq 2$
Pan et al. (2015)	Levee – Smooth - Impermeable	$R_c/H_{m0} < 0$
Gallach-Sanchez (2018)	Steep slopes and vertical - Smooth & artificial rough - Impermeable	$0 < R_c/H_{m0} \leq 3.25$
Ju et al. (2019)	Sloped - Smooth - Impermeable with berm	$0.5 < R_c/H_{m0} \leq 1.75$
Molines et al. (2019)	Breakwater - Rough - Permeable	$1.2 < R_c/H_{m0} \leq 4.78$
Mares-Nasarre et al. (2020)	Breakwater - Rough - Permeable	$0.33 < R_c/H_{m0} \leq 2.83$
Koosheh et al. (2022)	Seawall - Rough - Permeable	$0.75 < R_c/H_{m0} \leq 2.50$

The studies mentioned in Table 2.3 propose different formulas for q predictions, and P_{ov}, scale and shape factor calculations for obtaining V_{max} estimations. Three of these studies that have similar structure and test conditions to the current study are examined in detail for analysis of the results. Procedures for these studies are explained in detail in this section.

2.4.1 EurOtop (2018)

EurOtop (2018) provides extensive guidelines for calculating and assessing individual wave overtopping volumes. This method uses Equation (2.4) for mean wave overtopping rate calculation for rubble mound structure swith steep slopes (1:2 to 1:4/3). In Eurotop (2018) approach, maximum individual wave overtopping volume (V_{max}) is estimated using Equation (2.5) given below.

$$V_{max} = A \cdot \bar{V}[\ln(N_{ov})]^{1/b} \tag{2.5}$$

In Equation (2.6), N_{ov} is the number of the overtopping events depends on P_{ov} and number of waves (N), and $\bar{V}$ is the measured mean individual wave overtopping volume. The Weibull parameters, namely, the shape factor (b) and the scale factor (A) depending on b, are given in Equation (2.7) and Equation (2.8) respectively.

$$N_{ov} = N \cdot P_{ov} \tag{2.6}$$

$$b = 0.85 + 1500 \cdot Q^{*1.3} \tag{2.7}$$

$$A = \frac{1}{\Gamma\left(1 + \frac{1}{b}\right)} \tag{2.8}$$

Here, the probability of an individual wave overtopping event (P_{ov}) is calculated according to Equation (2.9). In calculations of Weibull parameters, non-dimensional mean overtopping discharge Q^* obtained with spectral mean wave period ($T_{m-1,0}$) (see Equation (2.10)) and mathematical gamma function (Γ) are used.

$$P_{ov} = \exp\left[-\left(\sqrt{-ln0.02}\frac{R_c}{R_{u2\%}}\right)^2\right] \tag{2.9}$$

$$Q^* = \frac{q}{q \cdot H_{m0} \cdot T_{m-1,0}} \tag{2.10}$$

Lastly, wave run-up ($R_{u2\%}$) is calculated by Equation (2.11) for 1:2 slopes to vertical walls according to the EurOtop (2018).

$$R_{u2\%} = 1.65 \cdot \gamma_b \cdot \gamma_f \cdot \gamma_\beta \cdot \zeta_{m-1,0} \cdot H_{m0}$$
With a maximum of
$$R_{u2\%} = 1.0 \cdot \gamma_f \cdot \gamma_\beta \left(4 - \frac{1.5}{\sqrt{\gamma_b \cdot \zeta_{m-1,0}}}\right) \tag{2.11}$$

2.4.2 Molines et. al (2019)

In this study, 164 2D physical experiments were carried out on conventional rubble mound breakwaters with a crown wall that has R_c/H_{m0} values ranging from 1.25 to 4.78 and H_{m0}/h values ranging from 0.10 to 0.32. These experiments were conducted under specific conditions, including non-breaking waves. Molines et al. identified disparities in the criteria used to select the number of overtopping events for fitting scale and shape factors, as identified by Pan et al. (2016). In their study, they compared the fitting of two parameters, A and b, in the Weibull distribution. They considered different percentages (10%, 30%, 50%, and 100% using a quadratic utility function) of the highest individual wave overtopping volumes. Utility functions were applied to account for the significance of observed data. When using the entire dataset with a quadratic utility function, all observations were utilized, with particular emphasis on the highest volumes.

For the V_{max} calculations (see Equation (2.12)), this study used q values obtained from the CLASH NN.

$$V_{max} = A \cdot \bar{V}[\ln(N_{ov} + 1)]^{1/b} \tag{2.12}$$

The shape and scale factors are calculated according to Equations (2.14) and (2.15) respectively. These equations were applied when employing the quadratic utility function for all observed individual wave overtopping volumes.

$$N_{ov} = N \cdot P_{ov} \tag{2.13}$$

$$b = 0.63 + 1.25 \cdot \exp(-3 \cdot 10^5 \cdot Q^*) \tag{2.14}$$

$$A = 1.4 - 0.4\frac{1}{b} \tag{2.15}$$

In this study, P_{ov} is calculated according to Equation (2.16). The shape factor was also expressed as a function of the dimensionless mean wave overtopping discharge,

Q^*. However, instead of spectral mean wave period ($T_{m-1,0}$), mean wave period (T_{01}) is taken into consideration in the Equation (2.17).

$$P_{ov} = \exp\left[-\left(\sqrt{-ln0.02}\frac{R_c}{R_{u2\%}}\right)^2\right] \quad (2.16)$$

$$Q^* = \frac{q}{q \cdot H_{m0} \cdot T_{01}} \quad (2.17)$$

According to the results of this study, the predictions for V_{max} based on above mentioned parameters generally matched well, except for the parameters fitted to the top 10% of individual wave overtopping volumes, which resulted in inaccurate overestimations when P_{ov}<0.01. Employing the top 10% of volumes to fit the Weibull distribution is only appropriate when N_{ov} is sufficiently large. Attempting to fit the statistical distribution with a low N_{ov} may result in less reliable predictions.

2.4.3 Mares-Nasarre et al. (2020

In this study, Mares-Nasarre et al. researched the impact of depth limited breaking wave conditions on individual overtopping volumes for rubble mound breakwaters with R_c/H_{m0} values ranging from 0.33 to 2.83 and H_{m0}/h values ranging from 0.2 to 0.9. They adopted the approach outlined by Molines et al. (2019) for 105 physical tests. Similarly, CLASH NN for q values and, Equation (2.12) for V_{max}, and lastly, Equation (2.17) for Q^* predictions are used. Then, they re-evaluated the Equations (2.14) and (2.15) for rubble mound breakwaters under breaking waves. The resulting outcomes for fitting the shape and scale factors are given in Equations (2.18) and (2.19) respectively.

$$b = 0.8 + \exp\left(-2 \cdot 10^5 \cdot Q^*\right) \quad (2.18)$$

$$A = 1.5 - 0.4\frac{1}{b} \quad (2.19)$$

According to the results of this study, the most accurate results for V_{max} predictions are obtained for Molines et al. (2019) whose method was developed for mound breakwaters with crown wall in non-breaking wave conditions. As a result, the impact of the depth-induced wave breaking on individual overtopping volumes may not be notable. Nonetheless, obtained Weibull parameter formulas are still viable within the tested ranges of R_c/H_{m0} and H_{m0}/h.

CHAPTER 3

METHODOLOGY

In this chapter, the methodology is described in detail. First the experimental setup is explained in Section 3.1, then the characteristics of the tested waves and design of the breakwater section are given in Sections 3.2 and 3.3 respectively. In Section 3.4, antifer placement methods used in experiments are described in detail. In Sections 3.5 and 3.6, measurement methods in order for waves and wave overtopping are described in depth. In Section 3.7, test conditions for experiments are mentioned.Lastly, in Section 3.8, analysis methods are explained for obtaining the results.

3.1 Experimental Setup

The physical model experiments were conducted in a 26.9 m long, 6.0 m wide and 1.0 m deep wave flume located in the Coastal and Ocean Engineering Laboratory of the Department of Civil Engineering, Middle East Technical University (METU). A 0.9 m wide inner channel was constructed in this wave flume and the rubble mound breakwater section was placed in this channel. The side view of the wave channel is given in Figure 3.1. As can be seen in Figure 3.1, there is a wave generator at one end of the wave channel, and passive wave absorbers at the other end to reduce wave reflection. In Figure 3.1, the coordinate system is set so that the x-direction points to the horizontal direction of the channel, the z-direction points to the vertical direction, and the starting point is placed at the point where the wave generator and the still water level meet.

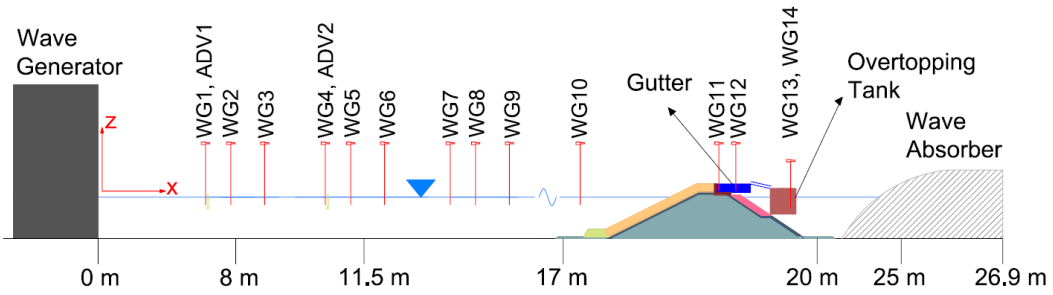

Figure 3.1 Wave flume

With the help of the wave gauges shown in Figure 3.1, water surface level and individual wave overtopping discharge were measured with a total of 14 wave gauges in different locations in the channel. The wave gauges placed in groups of three for irregular wave series measurements as WG1-WG2-WG3, WG4-WG5-WG6 and WG7-WG8-WG9 at shown intervals. Irregular wave series were analyzed using the method proposed by Mansard and Funke (1980) and the incident and reflected wave spectra were separated. The wave gauges in front of the structure (WG7-WG8-WG9) were positioned according to Klopman and van der Meer (1999).

In addition, video recordings taken during the experiments with two Sony RX0 cameras (Figure 3.2), which view the breakwater cross-section from the front (Figure 3.2 (a)) and from the side (Figure 3.2 (b)),

(a) Front camera view (b) Side camera view

Figure 3.2 Camera views from front (a) and side (b)

3.2 Wave Characteristics

As mentioned earlier a total of five irregular wave series are used in the physical model experiments. These wave series were generated using the JONSWAP spectrum (with a peak factor of γ=3.3). Table 3.1 shows the characteristics of the generated irregular wave series.

The wave steepness values given in Table 3.1 cover a wide range that can be seen in practical applications. The duration of the irregular wave series was targeted to be approximately 1000 waves as in similar studies. On the other hand, as can be seen from the calculated Irribaren numbers, it is predicted that the waves come to the breakwater without breaking and surging waves are predicted on the breakwater (EurOtop, 2018). This situation has been confirmed by observations in the experiments carried out. Again, as can be seen from the characteristic wave number given in Table 3.1, all the selected irregular waves have intermediate depth characteristics.

Table 3.1 Irregular wave series parameters

Parameers	**Irregular wave series 1 (W1)**	**Irregular wave series 2 (W2)**	**Irregular wave series 3 (W3)**	**Irregular wave series 4 (W4)**	**Irregular wave series 5 (W5)**
Spectral significant wave height, H_{m0} (m)	0.12	0.14	0.16	0.167	0.19
Peak wave period, T_p (s)	1.95	1.92	1.83	1.90	2.03
Spectral wave period, $T_{m-1,0}$ (s)	1.76	1.73	1.64	1.85	1.89
Wave steepness by spectral wave period, $s_{m-1,0}$	0.025	0.030	0.038	0,032	0,034
Irribaren number, $\xi_{m-1,0}$	3.17	2.88	2.57	2.80	2.71
Water depth, h (m)	0.49	0.49	0.49	0.49	0.49
h/H_{m0}	4.08	3.50	3.06	2.88	2.58

3.3 Breakwater Section Design

The section to be tested in the experiments was designed by considering the criteria recommended by AYGM (2016) for the design of a traditional single slope rubble mound breakwater. Accordingly, the dimensions of the antifer units to be used in the armor layer was based on the Hudson (SPM, 1984) approach based on the principle of depth-induced wave breaking. In the design of the section, the characteristics of five different irregular wave series were taken into consideration such that it was assumed that the sections would not be damaged, i.e. the armor unit sizes are overdesigned. The recommendations given by Frens (2007) on the effect of different placements of antifer units on cross-sectional stability were taken into consideration. Furthermore, viscosity induced effects were reduced by considering the method proposed by Burcharth et al. (1999) for core layer rock mass calculations. On the other hand, the method recommended by EurOtop (2018) was used for wave overtopping predictions depending on wave characteristics, the type of unit to be used in the armor layer of the breakwater and the height of the crown wall. The approach of Pedersen (1996) was used for the design of the crown wall, although the crown-wall was fixed during the experiments

The wave parameters used in the design are given in Table 3.1 for the five irregular wave series. As can be seen in Table 3.2, the unit dimensions corresponding to the highest wave height condition are selected and it was decided to use these dimensions in the sections. On the other hand, Table 3.3 shows two different crest elevations and accordingly two different relative crest elevations. As stated before, different crest heights will be tested for each test case. A close-up view of the breakwater section and the experimental setup is given in Figure 3.3.

Table 3.2 Breakwater section dimensions

Armor Layer Antifer Unit Weight (gr)	271
Filter Layer Rock Unit Weight (gr)	14-21
Core Layer Rock Unit Weight (gr)	1.4-7.1
Roughness Coefficient (EurOtop, 2018), γ_f	0.50
Crown Wall Crest Elevation, R_c (m)	0.153 ; 0.213
Breakwater Crest Elevation , A_c (m)	0.153

Table 3.3 Relative crest elevations

	Irregular wave series 1 (W1)	**Irregular wave series 2 (W2)**	**Irregular wave series 3 (W3)**	**Irregular wave series 4 (W4)**	**Irregular wave series 5 (W5)**
H_{m0}	0.12	0.14	1.60	0.167	0.19
R_c/H_{m0} R_c=0.153	1.28	1.09	0.96	0.92	0.85
R_c/H_{m0} R_c=0.213	1.78	1.52	1.33	1.28	1.18

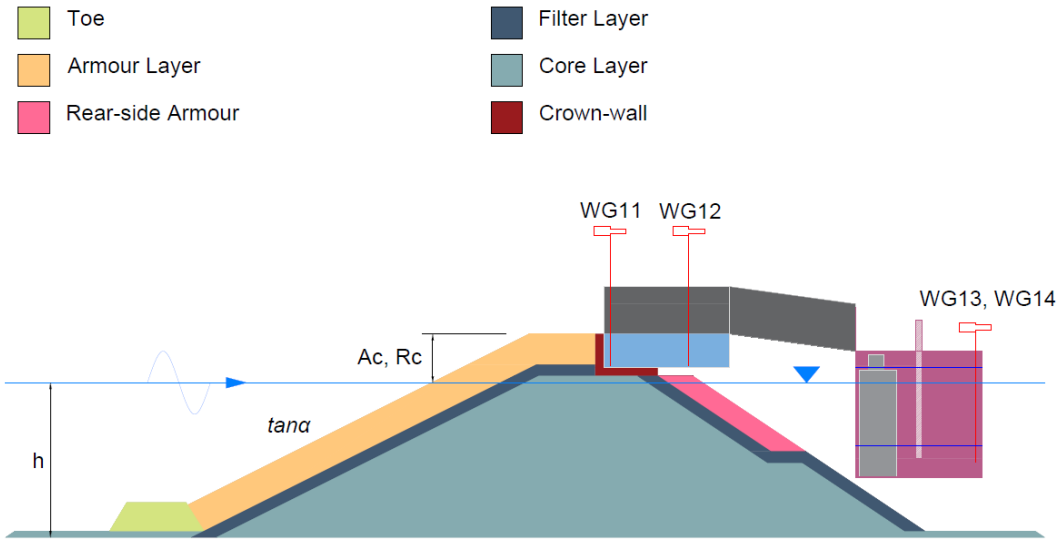

Figure 3.3 Breakwater section

The parameters of wave steepness, wave number, h/H_{m0}, Irribaren number and R_c/H_{m0} given in Table 3.1 are the main characteristics of the experiments on rubble mound breakwaters. The values chosen for these parameters in the present experiments are similar to those found in the literature for wave overtopping (e.g.

Koosheh et al., 2022). In other words, through the selected parameters, the compatibility of the current studies with similar experimental studies in the literature is ensured. Thus, the data that can be obtained from the studies in the literature can be compared with the data obtained in the existing experiments.

3.4 Antifer Placement Methods

During the experiments, four types of antifer placement methods are tested. These are closed pyramid, staggered closed pyramid and irregular placement methods. Each method were tested for two different packing density in order to observe its effect on wave overtopping. Brief information on placement methods and packing densites for each configuration are given in Table 3.4. More detailed information including armor layer thickness and unit spacing with top and side views of each configuration is given in Table 3.5.

Table 3.4 Antifer unit placements

Armor configuration name	Placement Method	Packing Density
CP1	Closed pyramid (CP)	54.80%
CP2	Closed pyramid (CP)	49.80%
DP1	Regular double pyramid (DP_{reg})	54.80%
DP2	Staggered double pyramid (DP_{stag})	54.80%
DP3	Staggered double pyramid (DP_{stag})	61.50%
DP4	Regular double pyramid (DP_{reg})	61.50%
IR1	Irregular (IR)	57.10%
IR2	Irregular (IR)	61.10%

3.4.1 Closed Pyramid Placement

The antifer-blocks are arranged in rows, following a specific pattern. In the first layer, these units are positioned with consistent horizontal spacing, maintaining a regular alignment with their grooves perpendicular to the slope. Moving on to the second layer, the blocks are placed diagonally in relation to the first row. They alternate direction, with some slanting to the left and others to the right, effectively

filling the gaps between the blocks of the first layer. Additionally, the blocks in the second layer are securely held in place by the blocks from the adjacent rows in the first layer, creating an integrated structure between the two layers. This arrangement forms a triangular shape, and the blocks in the second layer effectively seal the gaps in the first layer as shown in Table 3.5 (a and b).

3.4.2 Regular Double Pyramid and Staggered Double Pyramid Placements

Similar to the closed pyramid, first layer units are positioned with a regular alignment with fixed distances. However, in the second layer, units are placed over two first layer units with same spacing instead of in the gap between them as shown in Table 3.5 (c and f). This method results in an alternating placement in the horizontal direction that covers the filter layer completely.

For the staggered double pyramid method, second layer units are shifted half antifer length upwards along the armor layer plane as shown in Table 3.5 (d and e). As a result, an alternating placement in both directions is obtained and the through the gaps the filter layer can be seen.

3.4.3 Irregular Placement

The antifer units are arranged in rows without adhering to any specific pattern or strict positioning. Each block was individually dropped onto the slope from a short distance above. To achieve a consistent distribution of blocks with the desired level of packing density, it is essential to regulate the placement of the units. For this purpose, a standard grid is often used for the positioning or dropping of blocks in the first layer, based on the required number of blocks per unit area. As a result, this method provides a more controlled and uniform placement of the blocks to obtain the desired packing density. Examples of cross sections prepared with this method can be seen in Table 3.5 (g and h).

Table 3.5 Antifer unit placements and properties

(a) CP1 Placement Method

(a-1) CP1 placement, top view

(a-2) CP1 placement, side view

CP1 unit placement properties

X/D_n = 1.70, Y/D_n = 1.14, Armor layer thickness, t = 10.2 cm, γ_s = 54.8%

(b) CP2 Placement Method

(b-1) CP2 placement, top view

(b-2) CP2 placement, side view

CP2 unit placement properties

X/D_n = 1.87, Y/D_n = 1.09, Armor layer thickness, t = 9.5 cm, γ_s = 49.8%

(c) DP1 Placement Method

(c-1) DP1 placement, top view

(c-2) DP1 placement, side view

DP1 unit placement properties

X/D_n = 1.70 Y/D_n = 1.12, Armor layer thickness, t = 10.4 cm, γ_s = 54.8%

Tablo 5 (continued)

(d) DP2 Placement Method

(d-1) DP2 placement, top view

(d-2) DP2 placement, side view

DP2 unit placement properties

X/D_n = 1.70 Y/D_n = 1.12, Armor layer thickness, t = 10.4 cm, γ_s = 54.8%

(e) DP3 Placement Method

(e-1) DP3 placement, top view

(e-2) DP3 placement, side view

DP3 unit placement properties

X/D_n = 1.40 Y/D_n = 1.12, Armor layer thickness, t = 10.4 cm, γ_s = 61.5%,

(f) DP4 Placement Method

(f-1) DP4 placement, top view

(f-2) DP4 placement, side view

DP4 unit placement properties

X/D_n = 1.40 Y/D_n = 1.12, Armor layer thickness, t = 10.4 cm, γ_s = 61.5%

Tablo 5 (continued)

(g) IR1 Placement Method

(g-1) IR1 placement, top view

(g-2) IR1 placement, side view

IR1 unit placement properties
Armor layer thickness, t = 10.8 cm, γ_s = 57.1%

(h) IR2 Placement Method

(h-1) IR2 placement, top view

(h-2) IR2 placement, side view

IR2 unit placement properties
Armor layer thickness, t = 11 cm, γ_s = 61.1%

3.5 Wave Measurements

As mentioned, water surface level measurements are performed at 14 different points along the wave channel. The water surface level measurements along the channel are used to check that the selected waves are generated correctly. Irregular wave series were generated using the parameters given in Table 3.1. The water surface levels measured at wave gauge groups WG1-3, WG4-6 and WG7-9 were analyzed by the method of Mansard and Funke (1980) and the incident and reflected wave series were separated. The apparent wave height (H_{m0}), peak period (T_p), spectral wave period ($T_{m-1,0}$) and wave number (N) values of the targeted and measured incoming wave series are given comparatively in Table 3.1. As a result, no significant damage to the breakwater section was observed as targeted.

3.6 Overtopping Measurements

The methodology for wave overtopping measurements consists of the determination of individual wave overtopping values as accurately as possible, in line with the methods given in the literature, and the measurement of the total overtopping volume. In this section, the overtopping measurement systems to determine both mean overtopping discharges and individual overtopping volumes are described.

The method used by Koosheh et al. (2022) was taken as a basis for determining the individual wave overtopping rates. In this method, a total of four wave gauges are used, two on the overtopping gutter (WG11 and WG12, see Figure 3.3 a Figure 3.4) and two in the overtopping tank (WG13 and WG14, see Figure 3.3 and Figure 3.4 (a)).

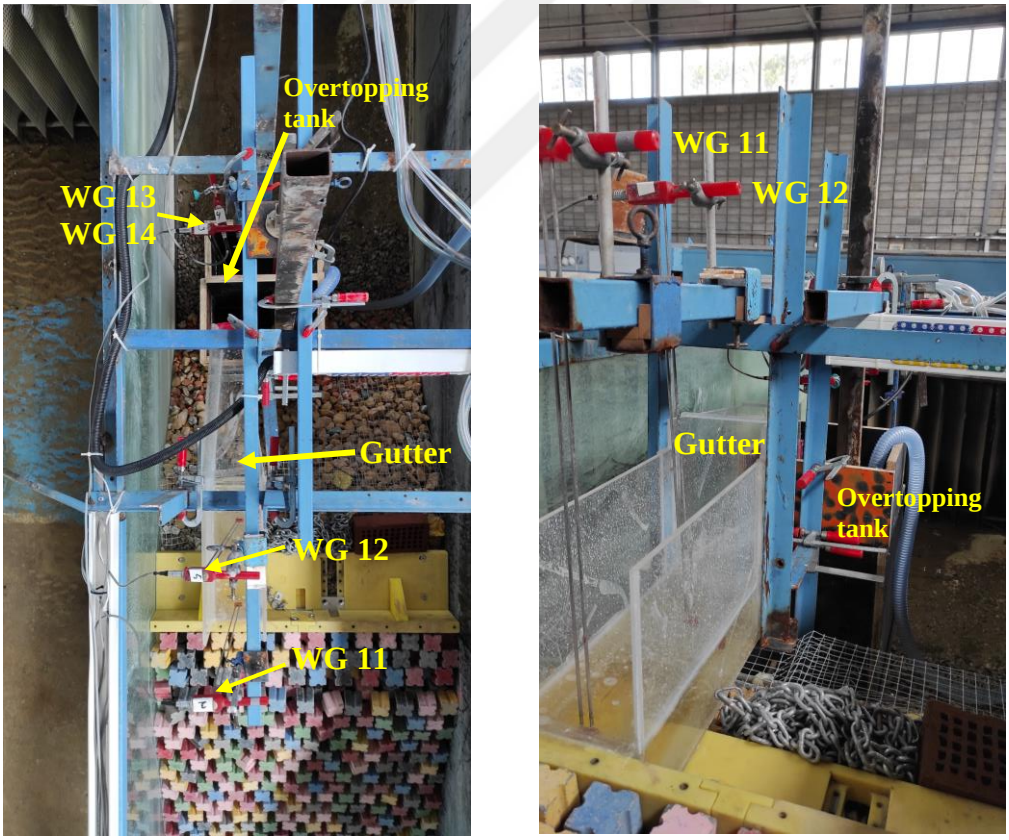

(a) Top view (b) Front view

Figure 3.4 Overtopping detection system

The width of the gutter is 15 cm, and the length is 30 cm. The gutter is placed at the same height as the crest level of the crown wall. The overtopping gutter consists of two parts, the lower part is a closed reservoir filled with water and the upper part is a gutter (see Figure 3.4 (b)). The wave gauges are immersed in the water reservoir about 10 cm through holes (see Figure 3.5). The wave gauges inside the gutter are used to determine the individual wave overtopping.

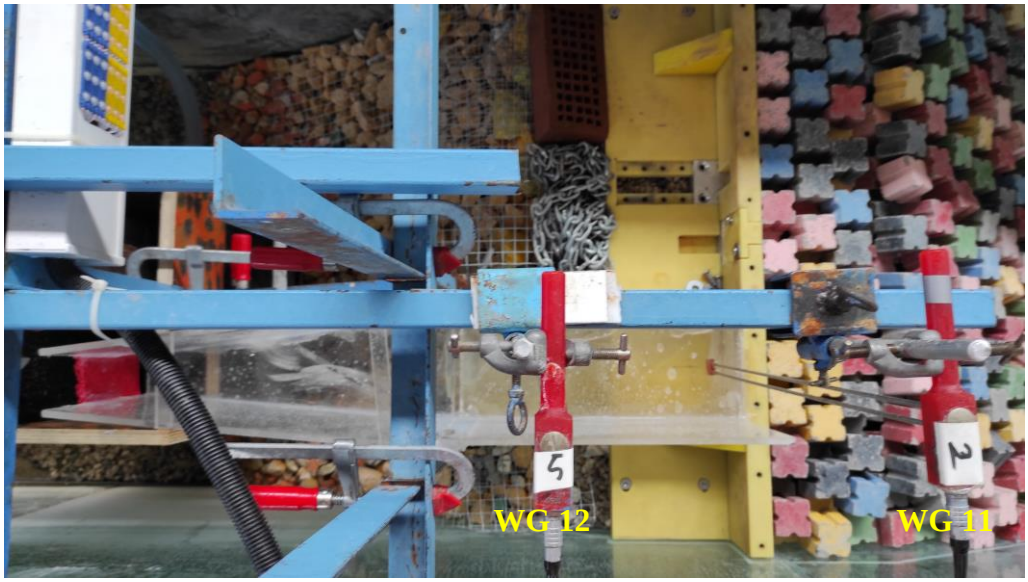

Figure 3.5 Overtopping gutter

The water from the gutter is then dropped into the overtopping tank through a narrowing channel (see Figure 3.6). The overtopping tank consists of two parts, the measuring tank and the drop tank. The two parts are separated by an impermeable wall starting about 10 cm above the bottom of the tank (see Figure 3.6). In the drop tank, a submersible pump with a constant cross-sectional area was used to stabilize the amount of water in the tank within a certain range (+10~35 cm from the tank bottom). The water drawn automatically by the pump at certain intervals is collected in a much larger collection tank outside the channel (see Figure 3.7) and at the end of the experiment, the amount of water collected in both tanks is measured with the help of a scale. Two wave gauges (WG13 and WG14) are positioned in the measurement tank. Each 1 cm rise observed by the wave gauges in the overtopping tank corresponds to an increase of 1 liter of water.

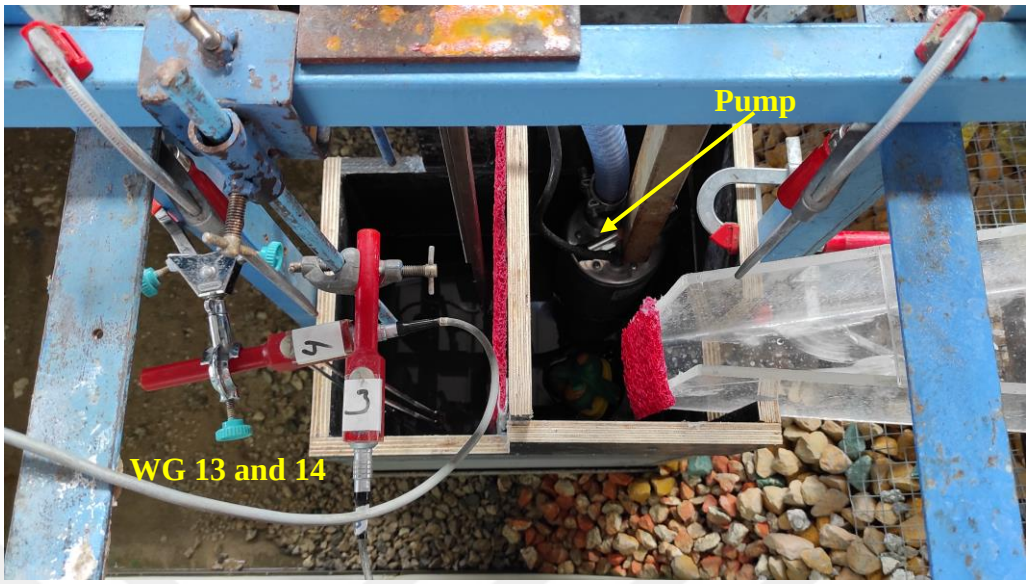

Figure 3.6 Overtopping tank

Figure 3.7 Overtopping collection tank

For the mean overtopping measurements, abovementioned total volume is taken into consideration. The mean wave overtopping discharge rates for a unit length (q_{mean} given with the unit of $m^3/s/m$) are obtained by dividing the total volume collected in the tank to the duration of the wave series and the width of the gutter (15 cm). The wave overtopping measurements were repeated twice for each armor layer configuration and each wave condition. Results of the mean wave overtopping measurements are used in analysis of γ_f that will be explained in detail in Section 4.1. Methodology for analysis of q_{mean} results are given in Section 3.8.2.

For individual wave overtopping measurements, first, in order to remove the vibrations caused by the falling water and, the noise caused by the data acquisition system in the water level change signals obtained from the wave gauges inside the drop tank (WG13 and WG 14), the signals obtained were first averaged and then a Butterworth type low-pass filter was applied on the average signal. A manual water level meter was also installed in the measuring tank for the pre-test calibration of the wave gauges in the measuring tank.

The individual wave overtopping rates are detected separately with the help of wave gauges on the gutter and wave gauges in the overtopping tank and then these individual wave overtopping events are correlated with each other. In addition, where necessary, for example in the case of very small wave overtopping flows or consecutive overtopping events, video recordings (Figure 3.8) taken during the experiments are used to verify the individual overtopping events detected from the signals.

(a) Front camera view (b) Side camera view

Figure 3.8 Overtopping event detected by cameras

In the detection of individual wave overtopping events by means of wave gauges on the gutter, the signals obtained are first cleaned from noise using the moving average method. Then, the signals are analyzed with the threshold cut-off method to obtain the start and end times of the overtopping events for both wave gauges. Separate threshold values are determined for each wave gauge and the times when these thresholds are exceeded and again when they fall below these thresholds are recorded. The prerequisite for the detection of an individual wave overtopping is that the threshold value is first exceeded at the wave gauge signal closer to the crown wall and then at the wave gauge signal closer to the tank. If the threshold is exceeded at both wave gauge signals, the difference of the times when the thresholds are exceeded is taken. If this time difference is less than half of the peak wave period of the wave condition and more than the time expressed by the following equation as dt_{min} (Equation (3.1)), this event is recorded as an individual wave overtopping event. In the equation c_d is the maximum wave celerity defined by L_{0p}/T_p, d_w is the distance between the two wave gauges, S_f is the sampling rate (which is 20 Hz in the present experiments).

$$dt_{min} = \max\left(\frac{d_w}{c_d}, \frac{1}{S_f}\right) \tag{3.1}$$

The individual overtopping events detected on the gutter are then correlated with the individual overtopping events detected with the help of the wave gauges in the tank. In order to detect individual wave overtopping events on the signal obtained from the wave gauges in the tank, the time dependent change of the signal (dV_{Tank}/dt) is firstly obtained. By applying the zero-up crossing method to this signal, the times when the change is positive (when the water in the tank increases) and the amount of increase during these time intervals are determined. In order to determine the individual wave overtopping flow rates that occur when the pump is working to stabilize the water level in the tank at a certain interval, the times when the pump starts to operate in the change signal are manually determined on the analysis code and the amount of the pump's flow rate is added to the change values in these intervals. In this way, individual overtopping amounts when the pump is running can

also be detected (Figure 3.9). In the final stage of the analysis, the individual overtopping events detected in the tank and the gutter are matched with each other and the false events obtained from the tank are eliminated.

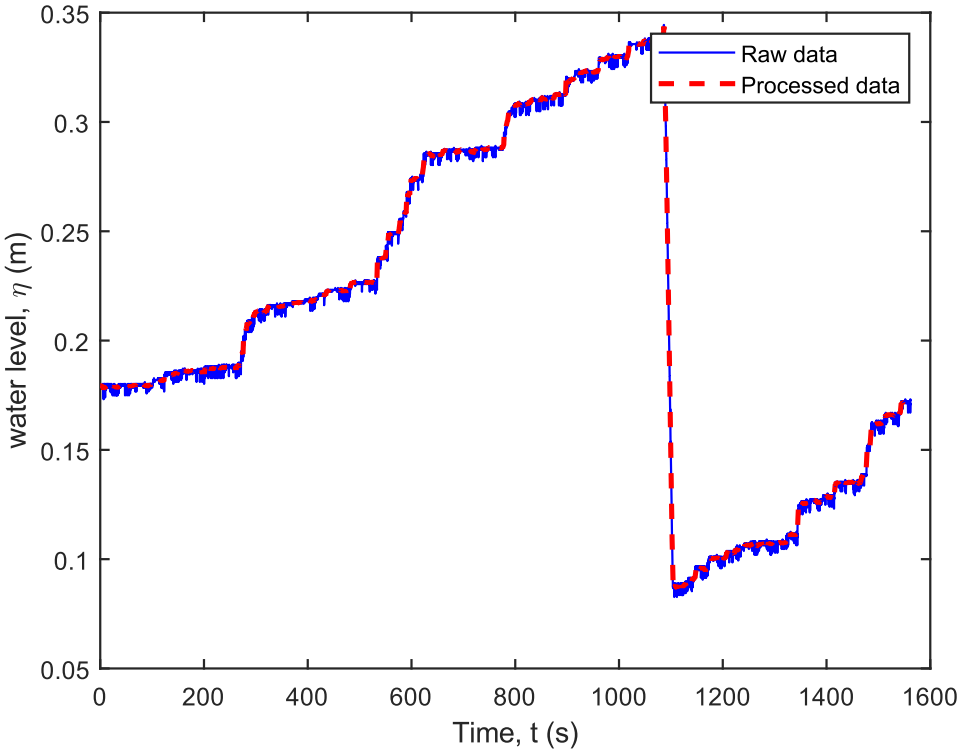

Figure 3.9 Water level change for WG13 and WG14

The condition for matching individual overtopping events from the tank and the gutter is that the individual overtopping events observed in the tank starts after the beginning of the events observed in the gutter (when the threshold value is exceeded in both wave gauge signals on the gutter) and before the start of the next event. If there is more than one tank-captured overtopping event between the start times of two consecutive events captured at the gutter, the larger of these overtopping values is taken into account and the others are ignored (see Figure 3.10). At the end of the matching process, individual overtopping events and values are obtained for the experiment. After the matching process, the individual overtopping volumes are summed and compared with the volume collected in the large overtopping collection

tank. In case of significant differences (>5%) between the two total volumes, the times of the individual overtopping series obtained are also verified with camera recordings.

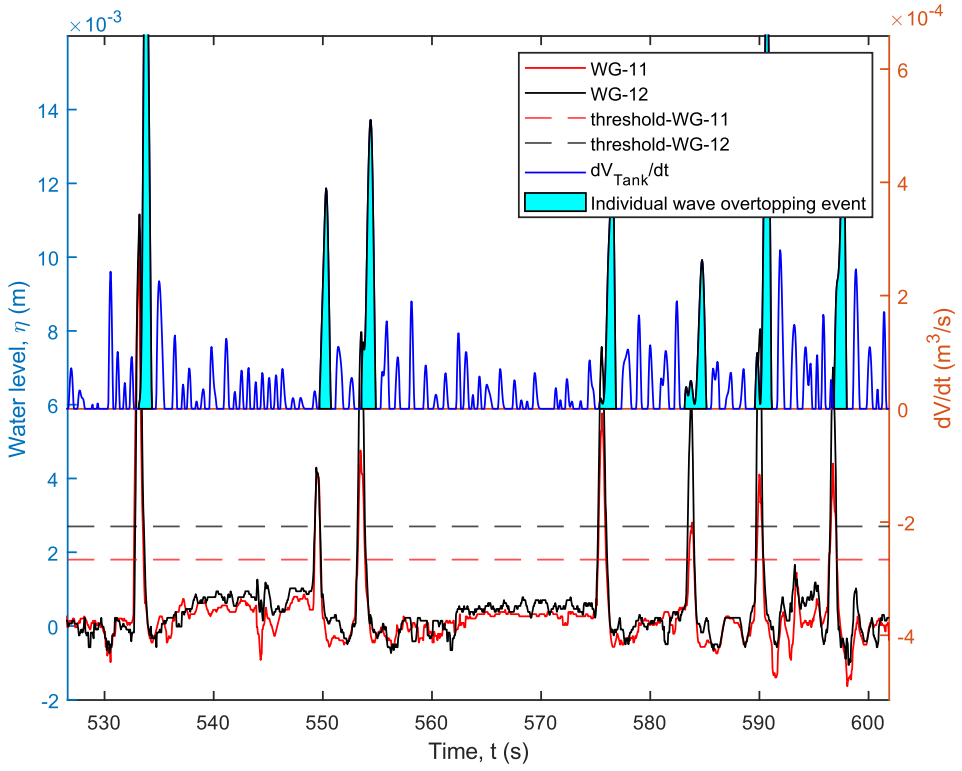

Figure 3.10 Individual wave overtopping analysis for CP2 placement method under W3 wave condition

3.7 Test Conditions

The scope of the experiments was determined as wave overtopping measurements under five different irregular wave series considering four different placements of antifer units; closed pyramid, double pyramid (regular and staggered), and irregular unit placement methods. Furthermore, these placement methods were investigated with two different packing densities each and two different crown wall crest heights. In total, 16 different combinations were studied under five different irregular wave series twice in order to create a data set.

3.8 Analysis Methods

In this section, the methods are explained for how the roughness coefficients are determined for different antifer placement techniques. Furthermore, the methods followed to analyze mean wave overtopping discharges and individual wave overtopping volumes are described based on the overtopping measurements.

3.8.1 Error Analysis

Two different error analysis methods, Mean Absolute Log Error (MALE), and Root Mean Square Log Error (RMSLE), While MALE measures the average of the logarithm of the absolute difference between calculated values and experimental values (Equation (3.2)), RMSLE is a measure that takes the square root of the average of the squared differences between of the logarithm of predicted and observed values (Equation (3.3)).

$$\text{MALE} = \frac{1}{N}\sum_{n=1}^{N}\left|log\left(\frac{P_n}{O_n}\right)\right| \tag{3.2}$$

$$\text{RMSLE} = \sqrt{\frac{1}{N}\sum_{n=1}^{N}\left(log\left(\frac{P_n}{O_n}\right)\right)^2} \tag{3.3}$$

Where P_n is the predicted values, O_n is the calculated values and N is the number ofthe data. These two methods are utilized in both determination of roughness coefficent and evaluation of overtopping results.

3.8.2 Determination of Roughness Coefficient

For roughness coefficient (γ_f) analysis, mean overtopping rate values obtained from the experiments were compared to the calculated values using EurOtop (2018) methodology (see Equation (2.4)). Two error analysis methods mentioned above were followed in order to obtain the γ_f value that yields the minimum error. Since both methods involve a trial-and-error process where the roughness coefficient was adjusted until the calculated error is minimized, an interval of roughness coefficient values for antifer units recommended by Bruce et al. (2009) (see Section 2.3.1**Error! Reference source not found.**) between 0.46-0.55 were checked for error analysis. Results for new roughness coefficients ($\gamma_{f,n}$) for three different placement methods (CP, DP, IR) and all methods combined are presented in Section 4.1.

3.8.3 Mean Wave Overtopping Discharge Analysis

For the analysis of mean wave overtopping discharges, first, $R_c/H_{m0} - q/\sqrt{g \cdot H_{m0}^3}$ graph is obtained in order to see the distiribution of the experimental results and the effects of placement method. Moreover, the effects of packing density on mean wave overtopping are also analysed according to $R_c/H_{m0} - q/\sqrt{g \cdot H_{m0}^3}$ graphs of each placement method. Second, comparison of measured (q_{meas}) and calculated (q_{calc}) values of mean wave overtopping is done according to Equation (2.4). Calculated values are obtained for both recommended roughness coefficient value (γ_f =0.5) for antifer units and placement methods by EurOtop (2018), and, different $\gamma_{f,n}$ values for each placement method proposed in Section 4.1. Resulting graphs and discussions are given in Section 4.2 for evaluation of the proposed roughness coefficents values on mean wave overtopping.

3.8.4 Individual Wave Overtopping Analysis

For the individual wave overtopping analysis, maximum individual volume (V_{max}) is the most important parameter that should be examined since an individual wave volume can differ much from mean overtopping discharge, thus, impacting the design. To do so, measured values according to the methods explained in Section 3.6, are compared to the results obtained according to the methods given in Section 2.4. The results for V_{max} are presented in non-dimensional form (V^*_{max}) according to Equation (3.4).Similar to the mean wave overtopping analysis, all methods are calculated for both roughness coefficients. The results and their discussions are given in Section 4.2.3. However, this study only focuses on the evaluation of the present methods, thus, no new formula for V_{max} predictions has been derived.

$$V_{max}^{*} = V_{max}/(g \cdot H_{m0} \cdot T_{01}^{2}) \tag{3.4}$$

CHAPTER 4

RESULTS

In this section, the outcomes of the analysis described in Section 3.7 are presented. The aim of this section is to objectively present and interpret the data collected, providing an understanding on the results of this study.

4.1 Roughness Coefficients

In this section, according to the error analysis methods explained in Section 3.8.1, $\gamma_{f,n}$ values obtained by minimizing RMSLE and MALE are presented for each placement method separately and all methods combined. Furthermore, the fit of new roughness coefficents to the experimental data is discussed. The effect of new roughness coefficent values for different antifer placement methods on mean wave overtopping prediction will be evaluated in the forthcoming Section 4.2.3.

In Table 4.1, error results for each placement method according to γ_f = 0.50 and $\gamma_{f,n}$ (which are selected based on the minimized the error metrics) error are given.

Table 4.1 Error analysis results for γ_f and $\gamma_{f,n}$

Placement method	γ_f	**MALE**	**RMSLE**
All	γ_f = 0.50	0.5843	0.7335
	$\gamma_{f,n}$ = 050	0.5843	0.7335
Regular Double Pyramid (DP_{reg})	γ_f = 0.50	0.6725	0.8614
	$\gamma_{f,n}$ = 0.54	0.5373	0.6618
Staggered Double Pyramid (DP_{stag})	γ_f = 0.50	0.5043	0.6573
	$\gamma_{f,n}$ = 0.52	0.4939	0.6064
Closed Pyramid (CP)	γ_f = 0.50	0.5362	0.6848
	$\gamma_{f,n}$ = 0.49	0.5284	0.6842
Irregular (IR)	γ_f = 0.50	0.6240	0.7471
	$\gamma_{f,n}$ = 0.48	0.5512	0.6946

The $\gamma_{f,n}$ value when the data from all the placement methods are combined agrees with EurOtop's (2018) suggested roughness coefficient value ($\gamma_{f,n}$ = γ_f = 0.50) (see Table 4.1). Moreover, the results agree with the CI range of Bruce et al. (2009) that is given in Table 2.1. However, investigating placement methods separately yields different results, as it can be seen in Table 4.1, as the roughness of the surface increse, roughness coefficient decreases.

In Figure 4.1 the non-dimensional values of measured mean overtopping discharges with respect to relative crest height are given. Furthermore, the calculations using the equation suggested by EurOtop (2018) Equation (2.4) are presented in the same figure using γ_f =1.0 (black dashed line) and γ_f =0.5 (solid line) with 90% upper and lower confidence bounds (red and blue dashed lines respectively).

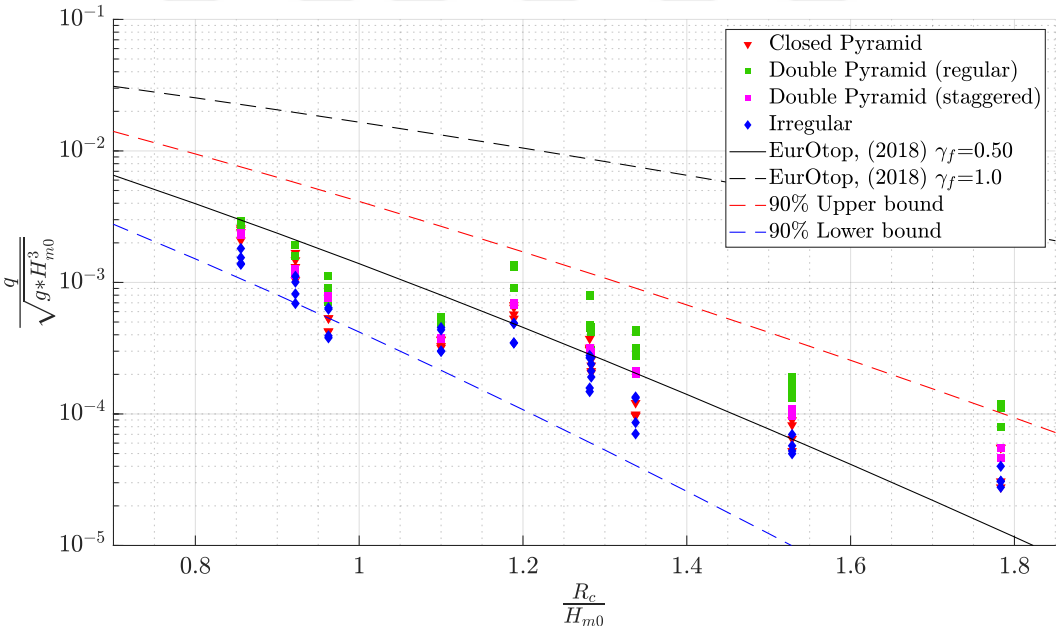

Figure 4.1 Distribution of mean wave overtopping discharges for all placement methods

As it can be seen from Figure 4.1, γ_f=0.50 provides a good fit overall, however, it underestimates where R_c/H_{m0}<1.09 and overestimates where R_c/H_{m0}>1.28. Moreover, when discharges are compared placement by placement, it significantly underestimates for two double pyramid methods for R_c/H_{m0}>1.09 and overestimates for IR for R_c/H_{m0}<1.33.

Through Figure 4.2 to Figure 4.5, distribution of non-dimensional mean overtopping discharges are given together with EurOtop (2018) curves calculated according to their respective γ_f and $\gamma_{f,n}$ values.

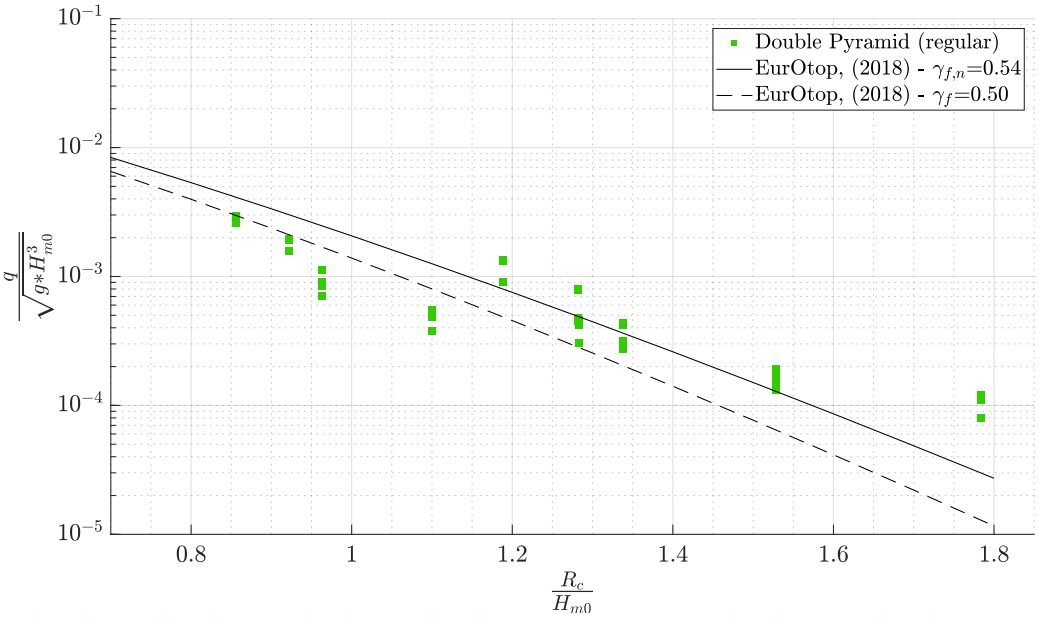

Figure 4.2 Distribution of mean wave overtopping discharges for DP_{reg} placement method

As the experimental results are the highest for DP_{reg} and shows most differnce from the EurOtop (2018) line (see Figure 4.1), roughness coefficient increases the most for this case. For DP_{reg} placement method, there is a 20% and 25% error reduction in for MALE and RMSLE respectively in favor of $\gamma_{f,n}$ according to Table 4.1. As it can be seen from Figure 4.2, using $\gamma_{f,n}$=0.54 provides a better fit overall, such that, the underestimation in higher R_c/H_{m0} portion (R_c/H_{m0}>1.28) of the graph is reduced significantly compared to increase in overestimation in lower R_c/H_{m0} portion (R_c/H_{m0}<1.09).

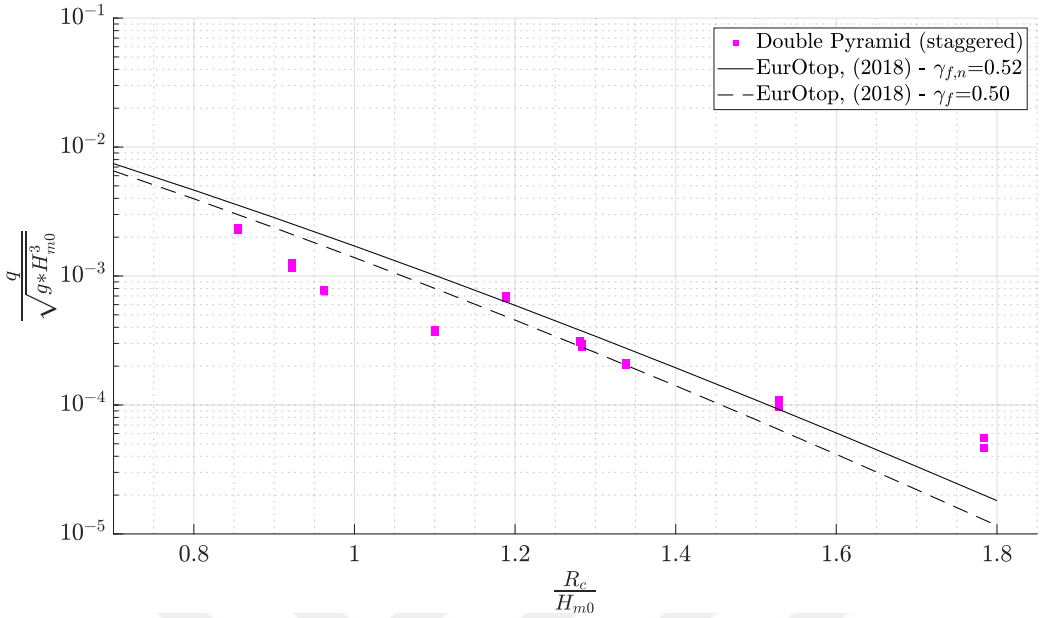

Figure 4.3 Distribution of mean wave overtopping discharges for DP_{stag} placement method

For DP_{stag} placement method, there is a 1% for MALE and 8% for RMSLE reduction in favor of $\gamma_{f,n}$ according to Table 4.1. Although the error reduction is smaller compared to DP_{reg}, Figure 4.3 shows that $\gamma_{f,n}$=0.52 results in a better fit overall for the whole range of R_c/H_{m0}.

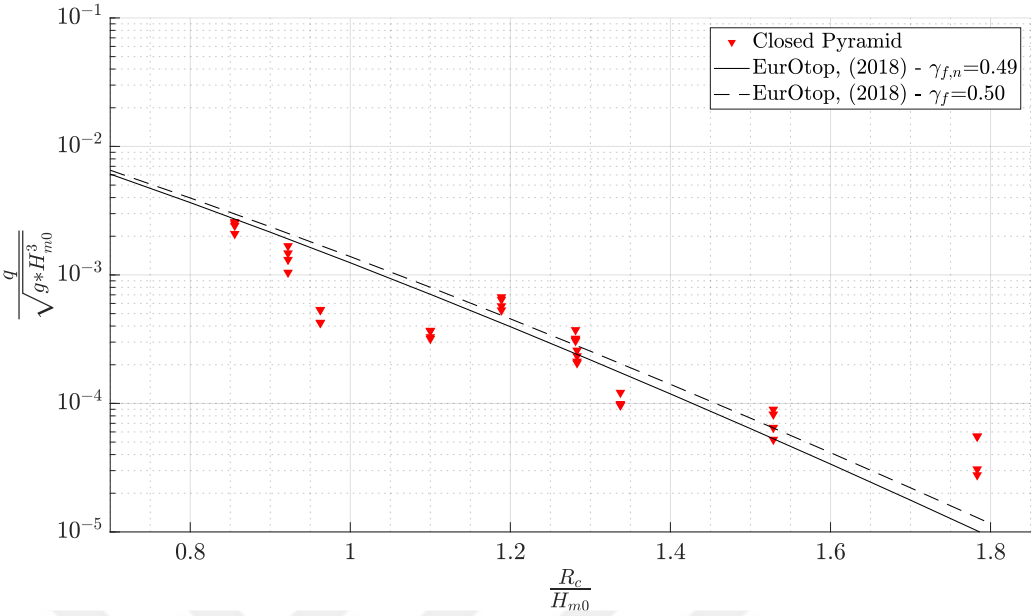

Figure 4.4 Distribution of mean wave overtopping discharges for CP placement method

For CP placement method, distribution of discharges is closest to the EurOtop (2018) line (see Figure 4.1 and Figure 4.4). This method that has regular gaps with a rough surface leads to having similar surface properties toboth DP and IR placements. Error analysis show the least reduction as MALE is reduced by less than 2% and RMSLE is almost identical for $\gamma_{f,n}$ (see Table 4.1). Although both γ_f values provides good fits for EurOtop (2018), according to lower MALE result $\gamma_{f,n}$ is selected as 0.49 that reduces overestimations in range of R_c/H_{m0}<1.33 and slightly increases underestimations in range of R_c/H_{m0}>1.52 (see Figure 4.4).

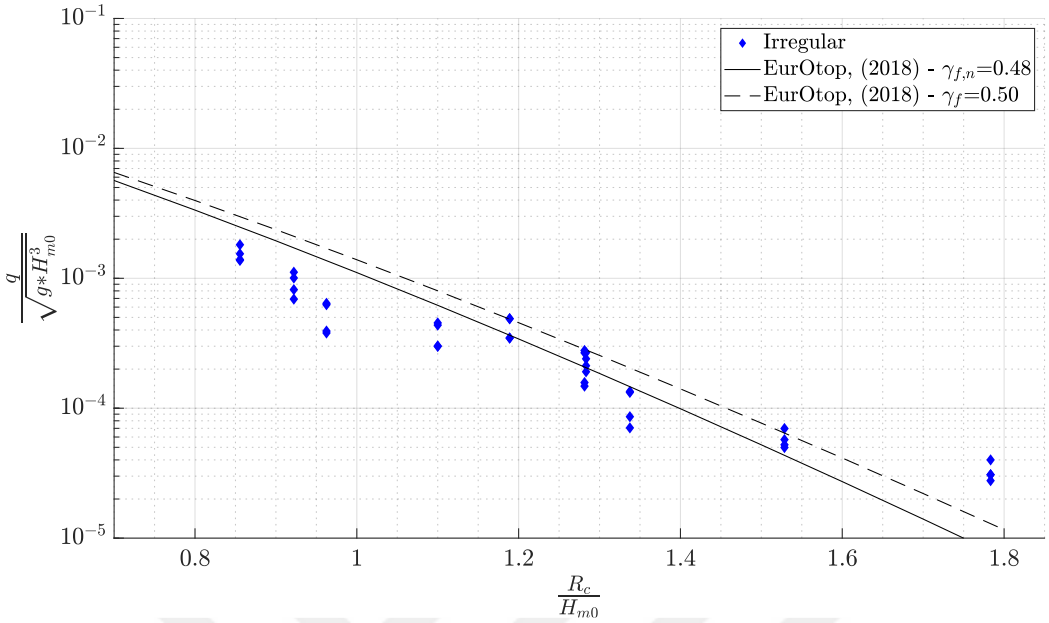

Figure 4.5 Distribution of mean wave overtopping discharges for IR placement method

For IR placement method, distribution of discharges is overestimated by the EurOtop (2018) line for γ_f=0.50 (see Figure 4.1 and Figure 4.5), due to this method having the roughest surface. As a result, $\gamma_{f,n}$ provides a better fit with an underestimation at R_c/H_m=1.78. Error analysis show around 10% reduction forboth MALE and RMSLE for $\gamma_{f,n}$ (see Table 4.1).

4.2 Mean Wave Overtopping

In this section, the effects of placement method (Section 4.2.1), packing density (Section 4.2.2) and newly proposed roughness coefficients (Section 4.2.1) on mean wave overtopping are discussed based on the experimental results.

4.2.1 Effect of Placement Method

In Figure 4.1 the results of mean overtopping discharges are given for all placement methods separately without considering the packing density changes. During the experiments, it was observed that having a flatter armor layer surface (less rough surface) increases the wave overtopping that directly impacts wave run-up and wave energy absorption.

As it can be seen in Figure 4.1, while the regular double pyramid method allowing most overtopping discharge, irregular method allows the least. The results shows that, there is around 50% reduction in mean overtopping discharges between them. Furthermore, IR allows 28% and 38% less mean overtopping discharge compared to CP and DP_{stag} placement methods respectively. On the other hand, CP yields 15% and 30% less overtopping discharge than DP_{reg} and DP_{stag} methods on average.

In Figure 4.6, comparison of mean wave overtopping discharges for two double pyramid methods is given in order to see the effect of the staggering of the second layer more clearly.

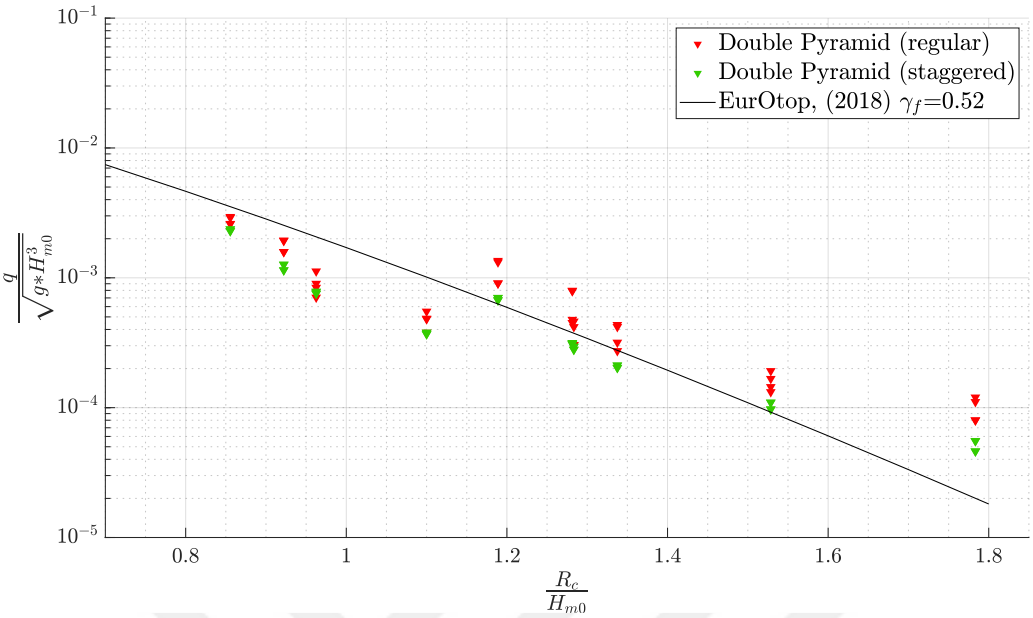

Figure 4.6 Distribution of mean wave overtopping discharges for DP_{reg} and DP_{stag} placement methods

For the staggered double pyramid method, gaps created by staggering the second layer reduces the dischargeas can be seen in Figure 4.6 , however, the smoother surface results in second most discarge amounts. Between two double pyramid placement methods, staggering the second layer reduces the mean overtopping discharge around 20% overall.

4.2.2 Effect of Packing Density

From Figure 4.7 to Figure 4.10, mean wave overtopping values for DP_{reg}, DP_{stag}, CP and IR placement methods are given respectively considering the packing density changes for different antifer placement methods.

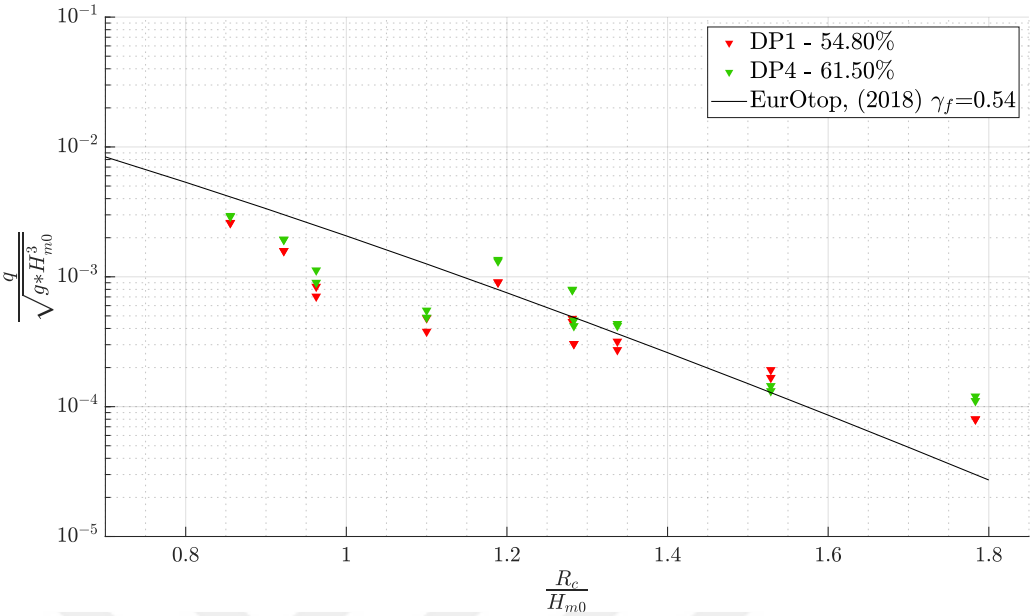

Figure 4.7 Distribution of mean wave overtopping of DP_{reg} placement method for two packing densities

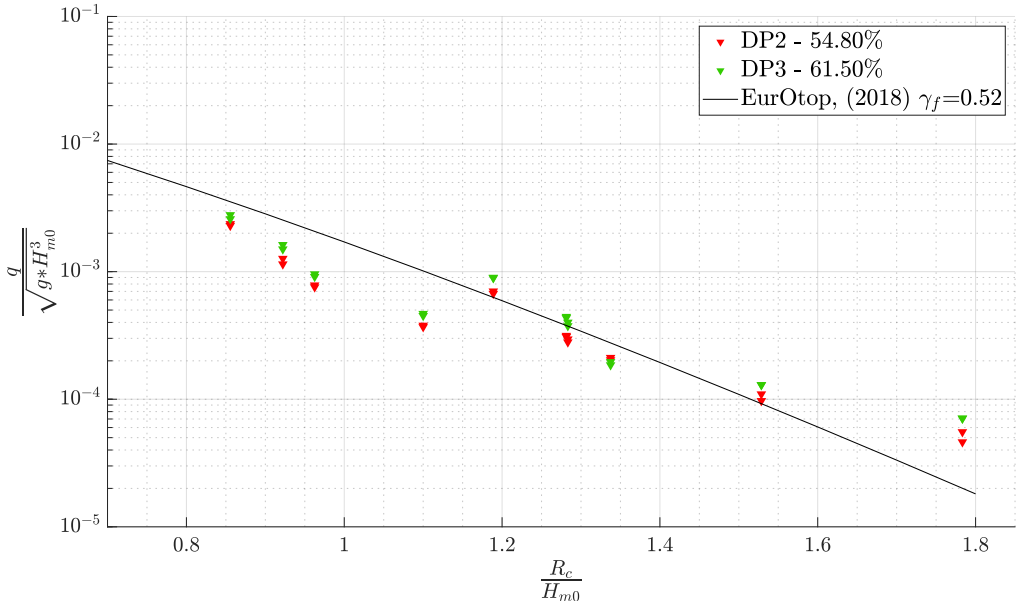

Figure 4.8 Distribution of mean wave overtopping of DP_{stag} placement method for two packing densities

Figure 4.7 and Figure 4.8 show clear results for the packing density – mean overtopping discharge relation for both DP placement methods.For DP_{reg}, only R_c/H_{m0} =1.52, and, for DP_{stag}, only R_c/H_{m0} =1.33 experiments out of ten yields higher discharge results for lower packing densities. As a result, it can be said that for both double pyramid placement methods, mean overtopping discharge increases with packing density. This situation is caused by the apparent reduction in gaps with the increasing packing density, waves found more surface area for run-up in DP placements.

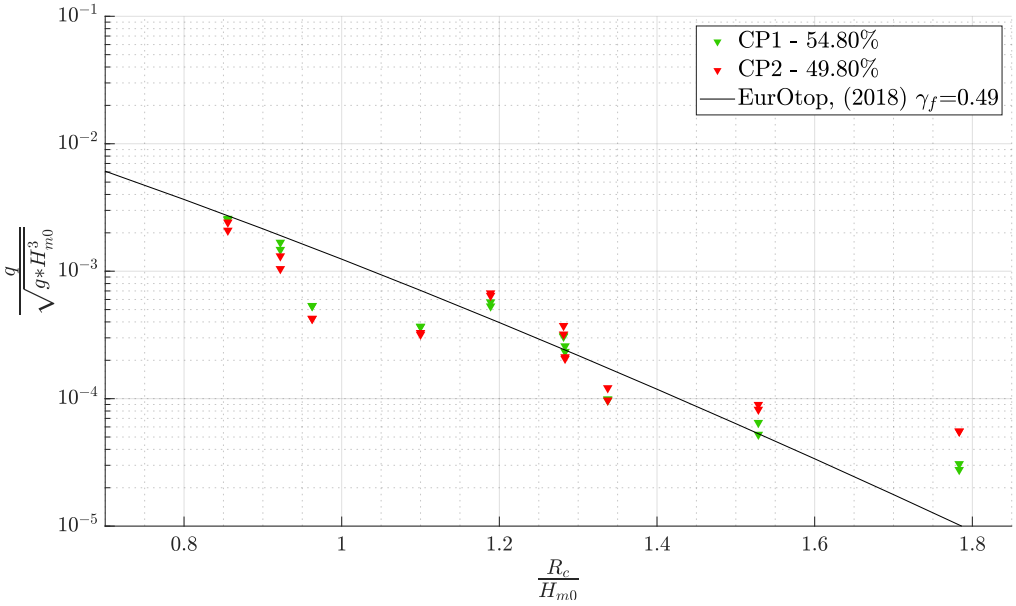

Figure 4.9 Distribution of mean wave overtopping of CP placement method for two packing densities

On the other hand, Figure 4.9 shows that for the lower half of the R_c/H_{m0} values ($0.85 \leq R_c/H_{m0} \leq 1.28$) yields higher q_{mean} values for higher packing density. This group also consists of experiments with $R_c=A_c$=0.153m given in Table 3.3. However, for the second half of the data, with R_c=0.213m ($1.18 \leq R_c/H_{m0} \leq 1.78$), lower packing density allows more overtopping discharge. As a result, for CP placement method, no clear correlation between packing density and mean overtopping discharge is observed.

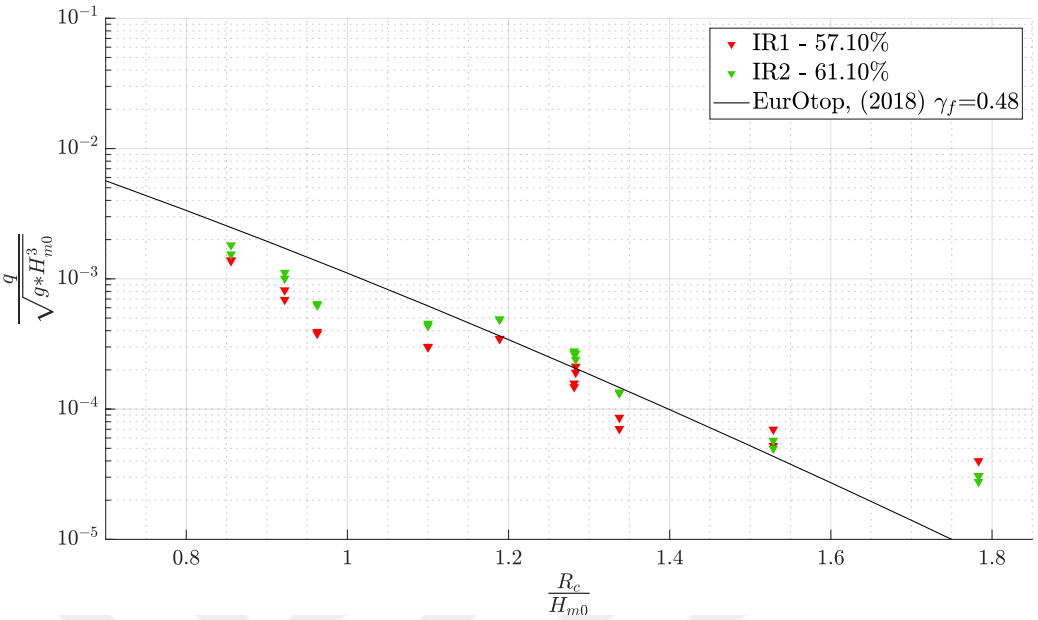

Figure 4.10 Distribution of mean wave overtopping of IR placement method for two packing densities

Lastly, for IR placement, eight out of ten R_c/H_{m0} sets shows similar results to DP placement results (see Figure 4.10) as the higher packing density allows more discharge. However, for higher R_c/H_{m0} values, this trend changes for the opposite and creates an uncertainity. Although, there seems to be a correlation between packing density and mean ovetopping discharge, IR placement method requires more observations with different packing densities for clearer results.

In conclusion, there is an effect of packing density, however, for some placement cases it is not apparent. The effect of packing density should be investigated with a larger data set where packking density changes. The analysis is completed in terms of placement method placement method changes considering that there should be scatter within each placement method as well.

4.2.3 Evaluation of the Effect of New Roughness Coefficients on Mean Wave Overtopping Prediction Methods

In this section, the effectiveness of roughness coefficients proposed in Table 4.1 for prediction of mean wave overtopping is discussed. For this purpose, two mean wave overtopping methods, EurOtop (2018) and CLASH NN, are compared with measured mean wave overtopping discharges during the experiments. First, the results for each placement method, then overall results are presented.

In Figure 4.11, dimensionless measured mean wave overtopping discharges (q^*_{meas}) are compared with dimensionless predicted mean wave overtopping discharges (q^*_{calc}) by EurOtop (2018) and CLASH NN according to both γ_f and $\gamma_{f,n}$ for DP_{reg} placement method. In Table 4.2, error analysis results of the data shown in, for both prediction methods and both roughness coefficient values.

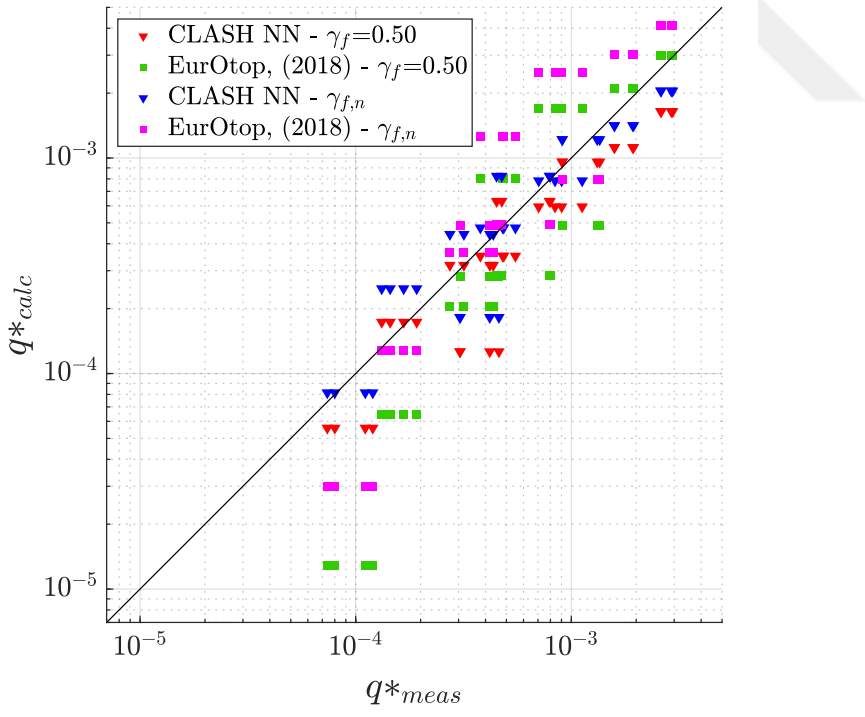

Figure 4.11 Comparison of measured and calculated mean wave overtopping discharges for DP_{reg} placement method

Table 4.2 Error analysis results for mean overtopping discharge prediction methods for DP_{reg} placement method

Prediction method	**Predicted *q***	**MALE**	**RMSLE**
EurOtop (2018)	q_{calc} with γ_f = 0.50	0.6726	0.8614
	q_{calc} with $\gamma_{f,n}$=0.49	0.5374	0.6619
CLASH NN	q_{calc} with γ_f = 0.50	0.4033	0.4959
	q_{calc} with $\gamma_{f,n}$=0.49	0.2859	0.3633

For DP_{reg} placement method, EurOtop (2018) method shows a scatter in Figure 4.11, such that, it overestimates for higher discharges and underestimates lower discharges for both γ_f and $\gamma_{f,n}$. On the other hand, CLASH NN yields a better scatter distributed around the line. This scatter comparison is supported by error results in Table 4.2. CLASH NN yields around 50% less MALE and around 45% less RMSLE than EurOtop (2018).

Although EurOtop (2018) has larger error, it can be seen that using $\gamma_{f,n}$ for q_{mean} prediction still reduces the error. Table 4.2 shows that MALE is reduced by 40% and RMSLE is reduced by about 20% when $\gamma_{f,n}$ is used instead of γ_f in mean overtopping discharge prediction. Similarly, CLASH NN also performs better when $\gamma_{f,n}$ is used, such that, MALE is reduced by 30% and RMSLE is reduced by 27%.

In Figure 4.12, q^*_{meas} are compared with q^*_{calc} according to EurOtop (2018) and CLASH NN and considering both γ_f and $\gamma_{f,n}$ for DP_{reg} placement method. In Table 4.3, error analysis results of the data shown in Figure 4.12, for both prediction methods and both roughness coefficient values.

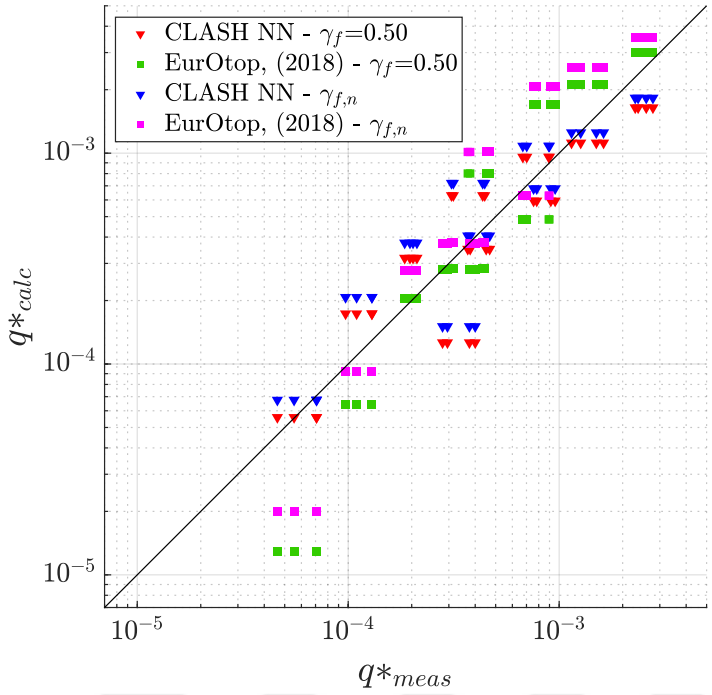

Figure 4.12 Comparison of measured and calculated mean wave overtopping discharges for DP_{stag} placement method

Table 4.3 Error analysis results for mean overtopping discharge prediction methods for DP_{stag} placement method

Prediction method	**Predicted *q***	**MALE**	**RMSLE**
EurOtop (2018)	q_{calc} with γ_f = 0.50	0.5044	0.6573
	q_{calc} with $\gamma_{f,n}$=0.49	0.4939	0.6065
CLASH NN	q_{calc} with γ_f = 0.50	0.3892	0.4684
	q_{calc} with $\gamma_{f,n}$=0.49	0.3945	0.4755

For DP_{stag} placement method, EurOtop (2018) method shows a scatter in Figure 4.12, similar to DP_{reg} (see Figure 4.11), such that, it overestimates for higher discharges and underestimates lower discharges for both γ_f and $\gamma_{f,n}$. On the other hand, CLASH NN yields a better scatter distributed around the line, however the scatter gets wider at lower discharges in Figure 4.12 relative to Figure 4.11. This scatter comparison is supported by error results in Table 4.2. CLASH NN yields around 25% less MALE and around 22% less RMSLE thanEurOtop (2018).

Although EurOtop (2018) has larger error, it can be seen that using $\gamma_{f,n}$ for q_{mean} prediction still reduces the error for DP_{stag} around 2% for MALE and 8% for RMSLE. On the other hand, CLASH NN yields higher error when $\gamma_{f,n}$ is used instead of γ_f, even though this increase is small, such that, both MALE and RMSLE are increased by 3%. This increase can be related to widening scatter in lower discharges mentiond earlier (see Figure 4.12).

In Figure 4.13, q^*_{meas} are compared with q^*_{calc} according to EurOtop (2018) and CLASH NN and considering both γ_f and $\gamma_{f,n}$ for CP placement method. In Table 4.4, error analysis results of the data shown in Figure 4.13, for both prediction methods and both roughness coefficient values.

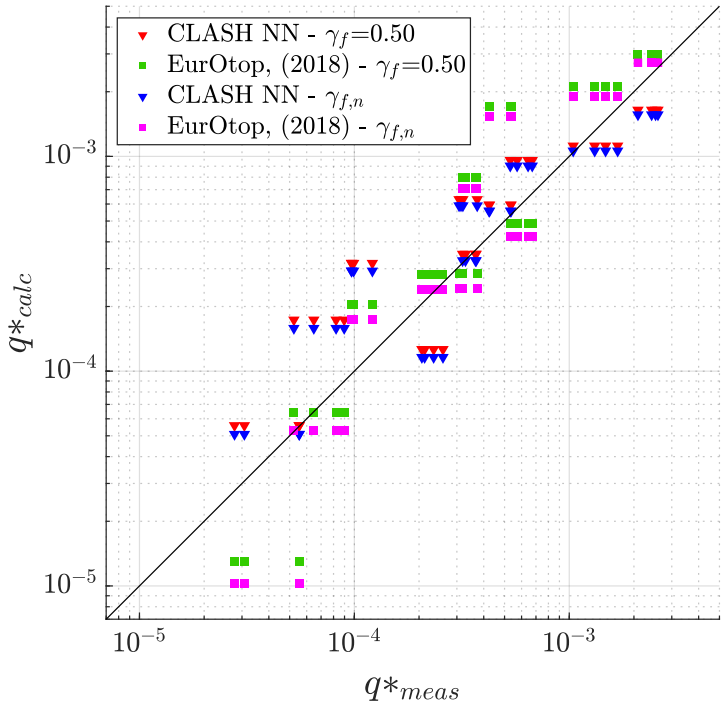

Figure 4.13 Comparison of measured and calculated mean wave overtopping discharges for CP placement method

Table 4.4 Error analysis results for mean overtopping discharge prediction methods for CP placement method

Prediction method	**Predicted *q***	**MALE**	**RMSLE**
EurOtop (2018)	q_{calc} with γ_f = 0.50	0.5363	0.6843
	q_{calc} with $\gamma_{f,n}$=0.49	0.5285	0.6848
CLASH NN	q_{calc} with γ_f = 0.50	0.4797	0.6024
	q_{calc} with $\gamma_{f,n}$=0.49	0.4284	0.5708

For CP placement method, in Figure 4.13, EurOtop (2018) method shows a better scatter with less underestimation for both γ_f and $\gamma_{f,n}$ in lower discharges than both DP placements (seeFigure 4.11 and Figure 4.12). On the other hand, CLASH NN yields a better scatter distributed around the line. This scatter comparison is supported by error results in Table 4.2. CLASH NN yields around 17% less MALE and around 20% less RMSLE than EurOtop (2018).

For CP placement method, EurOtop (2018) error does not change much when $\gamma_{f,n}$ is implemented for q_{mean} prediction, yet it still improves the prediction. The error reduces around 2% for MALE and RMSLE does not change. On the other hand, CLASH NN benefits from $\gamma_{f,n}$ compared to γ_f in mean overtopping discharge prediction such that, MALE is reduced by 10% and RMSLE is reduced by 5% according to Table 4.4.

In Figure 4.14, q^*_{meas} are compared with q^*_{calc} according to EurOtop (2018) and CLASH NN and considering both γ_f and $\gamma_{f,n}$ for IR placement method. In Table 4.5,error analysis results of the data shown in Figure 4.14, for both prediction methods and both roughness coefficient values.

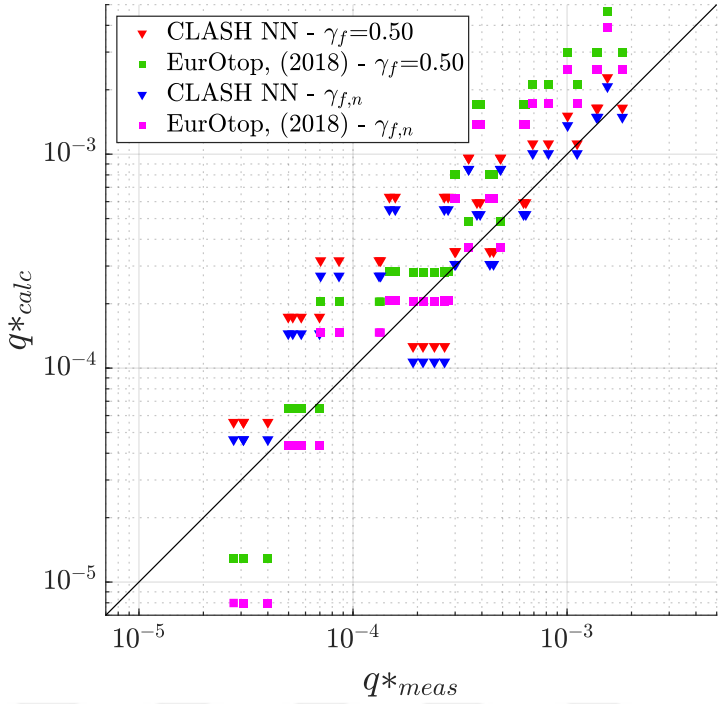

Figure 4.14 Comparison of measured and calculated mean wave overtopping discharges for IR placement method

Table 4.5 Error analysis results for mean overtopping discharge prediction methods for IR placement method

Prediction method	**Predicted *q***	**MALE**	**RMSLE**
EurOtop (2018)	q_{calc} with γ_f = 0.50	0.6241	0.7472
	q_{calc} with $\gamma_{f,n}$=0.49	0.5512	0.6947
CLASH NN	q_{calc} with γ_f = 0.50	0.6319	0.7570
	q_{calc} with $\gamma_{f,n}$=0.49	0.5597	0.6721

For IR placement method, in Figure 4.14, EurOtop (2018) method shows a scatter, such that, it overestimates for higher discharges and underestimates lower discharges for both γ_f and $\gamma_{f,n}$.. On the other hand, CLASH NN yields a better scatter distributed around the line, however the scatter gets wider at lower discharges in Figure 4.12. This scatter pattern resembles the DP_{stag}'s scatter in Figure 4.12. However, error results for this scatter are almost same between EurOtop (2018) and CLASHNN.

According to Table 4.5Table 4.2, the error difference between CLASH NN and EurOtop (2018) is around 2% less for both MALE and RMSLE.

On the other hand, for IR placement method, both prediction methods improve when $\gamma_{f,n}$ is used instead of γ_f in q_{mean} prediction. While EurOtop (2018) error decreases around 12% for MALE and 8% for RMSLE, CLASH NN error is reduced by %13 for MALE and 11% RMSLE according to Table 4.5.

In Figure 4.15, measured overtopping discharges are compared against values predicted with $\gamma_f = 0.50$ by Equation (2.4) and CLASH NN. Similarly, in Figure 4.16, results of same procedure calculated with $\gamma_{f,n}$ are presented. In Table 4.6, error analysis results of the data shown in Figure 4.15 and Figure 4.16 are given, for both prediction methods and both roughness coefficient values.

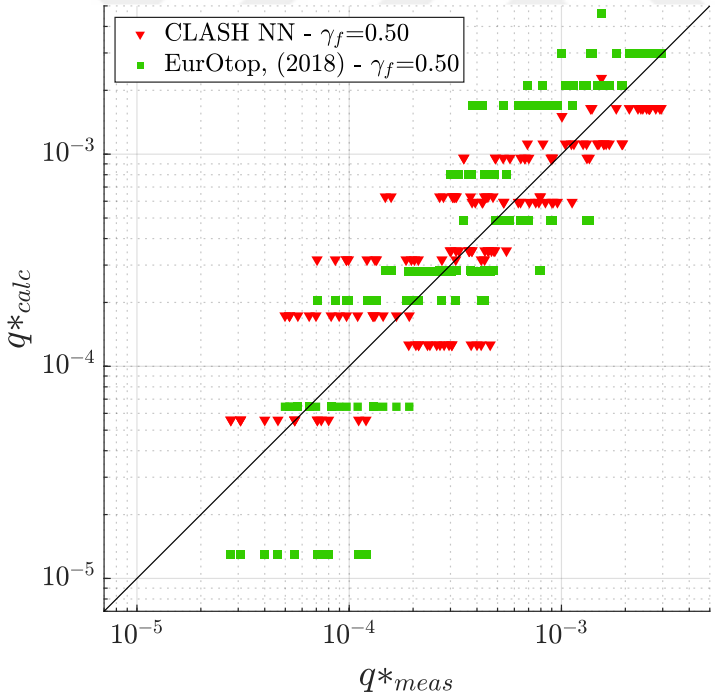

Figure 4.15 Comparison of measured and calculated (with $\gamma_f = 0.50$) mean wave overtopping discharges

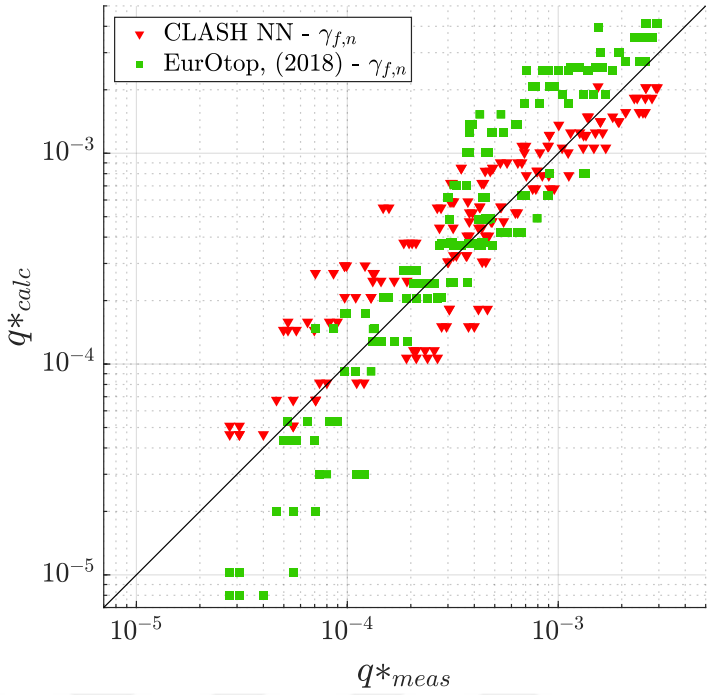

Figure 4.16 Comparison of measured and calculated (with $\gamma_{f,n}$) mean wave overtopping discharges

Table 4.6 Error analysis results for mean overtopping discharge prediction methods

Prediction method	**Predicted *q***	**MALE**	**RMSLE**
EurOtop (2018)	q_{calc} with γ_f = 0.50	0.5843	0.7417
	q_{calc} with $\gamma_{f,n}$	0.5277	0.6628
CLASH NN	q_{calc} with γ_f = 0.50	0.4797	0.5919
	q_{calc} with $\gamma_{f,n}$	0.4284	0.5328

In both figures, it can be seen that EurOtop (2018) and CLASH NN has similar scatter and provides accurate predictions compared to EurOtop (2018). Moreover, for both prediction methods, scatter further decreases in Figure 4.16. However, EurOtop (2018) slightly underestimates in lower discharges and slightly overestimates in higher discharges for both γ_f and $\gamma_{f,n}$. On the other hand, CLASH NN has a higher scatter,thus less accuracy at lower discharges, yet it gets more accurate at higher discharges when for both $\gamma_{f,n}$ is used.

Although CLASH NN yields lower error overall (see Table 4.6**Error! Reference s ource not found.**), EurOtop (2018) and CLASH NN methods yields better scatters on different ranges compared to each other as can be seen in Figure 4.16, such that, while CLASH NN's scatter is distributed closer to the line at higher discharges, EurOtop's (2018) scatter looks better at middle values, and both methods getless accurate at smaller discharges.

Furthermore, Table 4.6 shows that, utilizing newly proposed roughness coefficent values for mean wave overtopping discharge prediction yields more accurate results for all cases. For all placement methods combined, Table 4.6 shows that EurOtop's (2018) MALE and RMSLE are both reduced by 11% when $\gamma_{f,n}$ is used instead of γ_f in mean overtopping discharge prediction. Similarly, CLASH NN also performs better when $\gamma_{f,n}$ is used, such that, MALE and RMSLE are both reduced by 11% as well.

Lastly, the effect of $\gamma_{f,n}$ will be further discussed in Section 4.2.3, since q_{mean} estimation is a crutial step for V_{max} predictions in individiual wave overtopping analysis.

4.3 Individual Wave Overtopping

In this section, the effects of placement method (Section 4.3.1), packing density on individual wave overtopping volumes and evaluation of individual wave overtopping volume prediction methods (Section 4.3.2) are discussed based on the experimental results.

4.3.1 Efefct of Placement Method

In Figure 4.17, the results of maximum individual wave overtopping volumes are given for all placement methods separately.

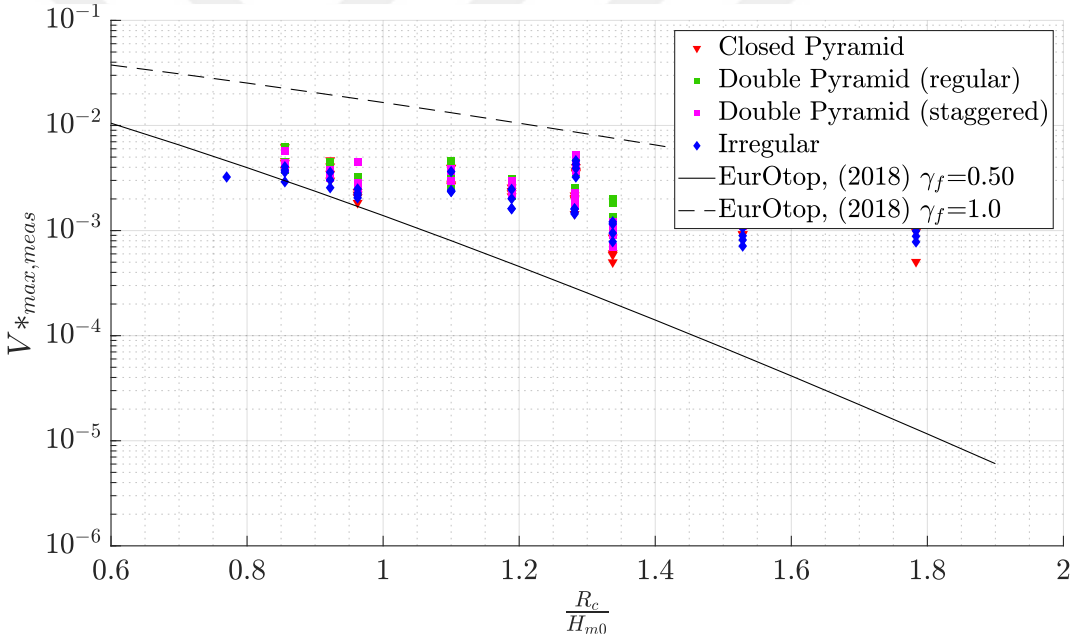

Figure 4.17 Distribution of maximum individual wave overtopping volumes for all placement methods

As it can be seen from Figure 4.17, maximum individual overtopping volumes differ from mean wave overtopping discharges. While mean wave overtopping discharges were scattered around the EurOtop (2018) line for γ_f=0.5 line (See Figure 4.1), maximum overtopping volumes are much higher.On average, maximum individual overtopping volumes are around 45% higher than mean overtopping discharges.

As it can be seen in Figure 4.17, while the regular double pyramid method allowing most maximum individual overtopping volume, irregular method allows the least. The results shows that, there is around 30% reduction in maximum individual overtopping volumes between them. Furthermore, IR allows 12% and 22% less maximum individual overtopping volumes compared to CP and DP_{stag} placement methods respectively. On the other hand, CP yields 11% and 20% less maximum individual overtopping volume than DP_{reg} and DP_{stag} methods on average. Between two double pyramid placement methods, staggering the second layer reduces the maximum individual overtopping volume around 10% overall.

4.3.2 Evaluation of Individual Wave Overtopping Volume Prediction Methods

In this section, the effectiveness of V_{max} prediction methods are compared within the framework given in Section 3.8.4 are discussed. For this purpose, three V_{max} prediction methods, EurOtop (2018), Molines et al. (2019) and Mares-Nasarre et al. (2020), are compared with measured maximum individual overtopping volumes during the experiments. First, the results for each placement method, then overall results are presented and commented.

In Figure 4.18 and Figure 4.19, dimensionless measured maximum overtopping volumes ($V^*_{max,meas}$) are compared with dimensionless predicted mean maximum overtopping volumes ($V^*_{max,calc}$) by EurOtop (2018), Molines et al. (2019) and Mares-Nasarre et al. (2020) according to both γ_f (see Figure 4.18) and $\gamma_{f,n}$ (see Figure 4.19) for DP_{reg} placement method. In Table 4.7, error analysis results of the data shown in Figure 4.18 and Figure 4.19, for both roughness coefficient values respectively, and for all prediction methods.

Table 4.7 Error analysis results for maximum individual overtopping volume prediction methods for DP_{reg} placement method

Prediction method	**Predicted *q***	**MALE**	**RMSLE**
EurOtop (2018)	q_{calc} with γ_f = 0.50	1.5249	1.9052
	q_{calc} with $\gamma_{f,n}$=0.54	1.1609	1.5344
Molines et al. (2019)	q_{calc} with γ_f = 0.50	0.4636	0.6774
	q_{calc} with $\gamma_{f,n}$=0.54	0.4200	0.5618
Mares-Nasarre et al. (2020)	q_{calc} with γ_f = 0.50	0.4569	0.6762
	q_{calc} with $\gamma_{f,n}$=0.54	0.4278	0.5938

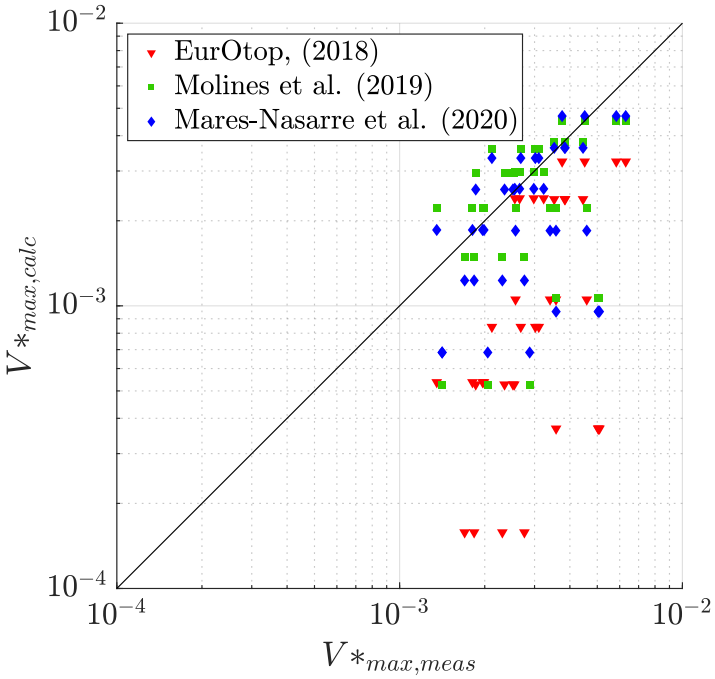

Figure 4.18 Comparison of measured and calculated maximum individual overtopping volumes for DP_{reg} placement method (q_{calc} is predicted with γ_f = 0.50)

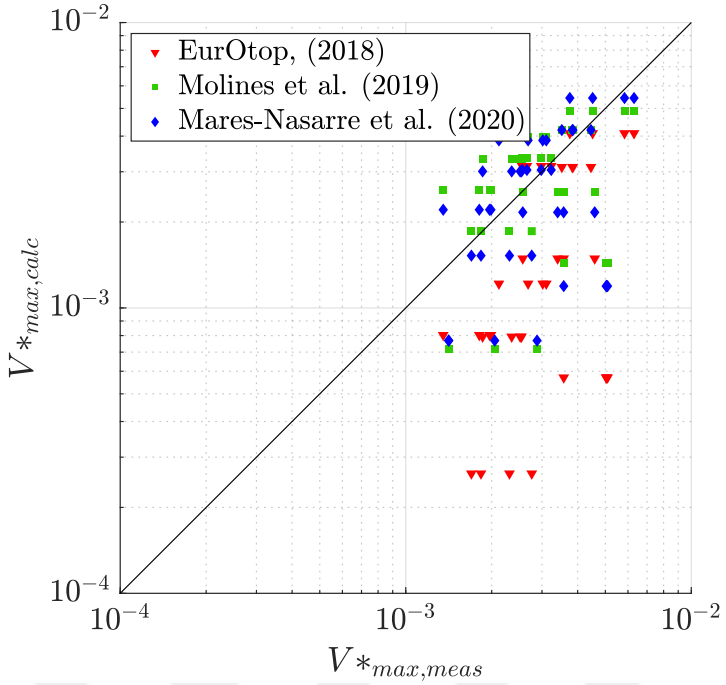

Figure 4.19 Comparison of measured and calculated maximum individual overtopping volumes for DP_{reg} placement method (q_{calc} is predicted with γ_{fn})

For DP_{reg} placement method, EurOtop (2018) heavily underestimates $V*_{max}$ predictions as it can be seen from Figure 4.18 and Figure 4.19, for γ_f and $\gamma_{f,n}$ respectively, thus yields large error results for both MALE and RMSLE (see Table 4.7).

On the other hand, Molines et al. (2019) and Mares-Nasarre et al. (2020) yield better and relatively close scatters in Figure 4.18 and Figure 4.19. This scatter comparison is supported by error results in Table 4.7. The error difference between Molines et al. (2019) and Mares-Nasarre et al. (2020) is under 2% for both MALE and RMSLE.

Although EurOtop (2018) has larger error, it can be seen that using $\gamma_{f,n}$ for q_{mean} prediction still reduces the error for $V*_{max}$ prediction. Table 4.7 shows that MALE is reduced by 24% and RMSLE is reduced by about 20% when $\gamma_{f,n}$ is used instead of γ_f in maximum overtopping volume prediction.

For Molines et al. (2019) also performs better when $\gamma_{f,n}$ is used, such that, MALE is reduced by 9% and RMSLE is reduced by 17%. Similarly, for Mares-Nasarre et al.

(2020) MALE is reduced by 7% and RMSLE is reduced by 12% when $\gamma_{f,n}$ is used in maximum overtopping volume prediction (see Table 4.7).

In Figure 4.20 and Figure 4.21, $V^*_{max,meas}$ are compared with $V^*_{max,calc}$ by EurOtop (2018), Molines et al. (2019) and Mares-Nasarre et al. (2020) according to both γ_f (see Figure 4.20) and $\gamma_{f,n}$ (see Figure 4.21) for DP_{stag} placement method. In Table 4.8, error analysis results of the data shown in Figure 4.20 and Figure 4.21, for both roughness coefficient values respectively, and for all prediction methods.

Table 4.8 Error analysis results for maximum individual overtopping volume prediction methods for DP_{stag} placement method

Prediction method	**Predicted *q***	**MALE**	**RMSLE**
EurOtop (2018)	q_{calc} with γ_f = 0.50	1.3760	1.7667
	q_{calc} with $\gamma_{f,n}$=0.52	1.1821	1.5762
Molines et al. (2019)	q_{calc} with γ_f = 0.50	0.5088	0.6714
	q_{calc} with $\gamma_{f,n}$=0.52	0.4948	0.6317
Mares-Nasarre et al. (2020)	q_{calc} with γ_f = 0.50	0.4814	0.6499
	q_{calc} with $\gamma_{f,n}$=0.52	0.4831	0.6258

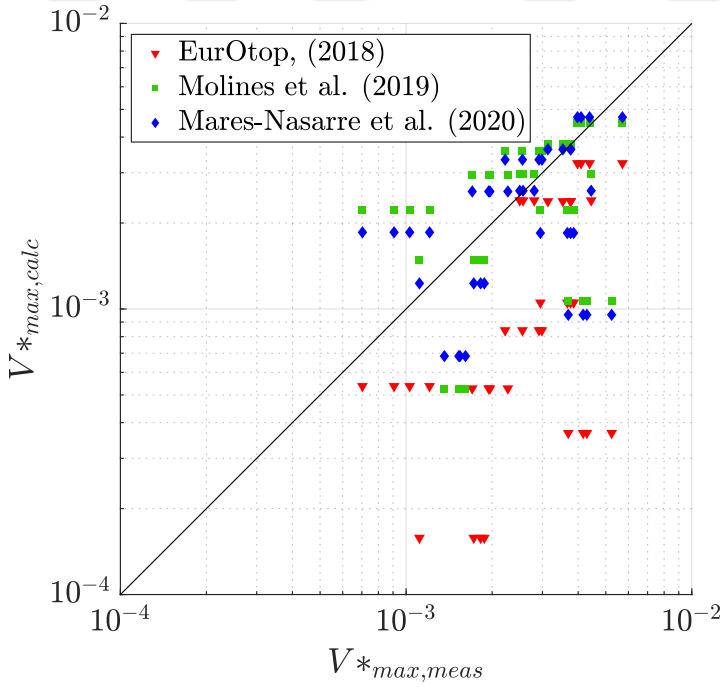

Figure 4.20 Comparison of measured and calculated maximum individual overtopping volumes for DP_{stag} placement method (q_{calc} is predicted with γ_f = 0.50)

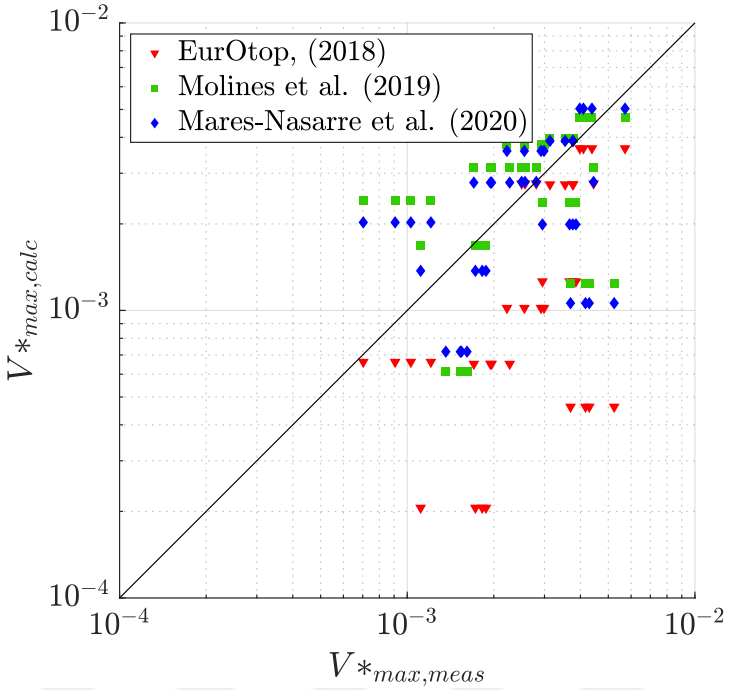

Figure 4.21 Comparison of measured and calculated maximum individual overtopping volumes for DP_{stag} placement method (q_{calc} is predicted with $\gamma_{f,n}$)

For DP_{stag} placement method, EurOtop (2018), again, heavily underestimates $V*_{max}$ predictions as it can be seen from Figure 4.20 and Figure 4.21, for γ_f and $\gamma_{f,n}$, thus yields large error results for both MALE and RMSLE (see Table 4.7).

Molines et al. (2019) and Mares-Nasarre et al. (2020) yield better and relatively close scatters in Figure 4.20 and Figure 4.21. This scatter comparison is supported by error results in Table 4.8. The error difference between Molines et al. (2019) and Mares-Nasarre et al. (2020) is under 5% for both MALE and RMSLE.

Although EurOtop (2018) has larger error, it can be seen that using $\gamma_{f,n}$ for q_{mean} prediction still reduces the error for $V*_{max}$ prediction. Table 4.8Table 4.2 shows that MALE is reduced by 15% and RMSLE is reduced by about 11% when $\gamma_{f,n}$ is used instead of γ_f in maximum overtopping volume prediction.

For Molines et al. (2019), although error differences are small, also performs better when $\gamma_{f,n}$ is used, such that, MALE is reduced by 2% and RMSLE is reduced by 6%.

Similarly, for Mares-Nasarre et al. (2020) MALE is almost the same and RMSLE is reduced by 4% when $\gamma_{f,n}$ is used in maximum overtopping volume prediction instead of γ_f (see Table 4.8).

In Figure 4.22 and Figure 4.23, $V^*_{max,meas}$ are compared with $V^*_{max,calc}$ by EurOtop (2018), Molines et al. (2019) and Mares-Nasarre et al. (2020) according to both γ_f (see Figure 4.22) and $\gamma_{f,n}$ (see Figure 4.23) for CP placement method. In Table 4.9Table 4.7, error analysis results of the data shown in Figure 4.22 and Figure 4.23, for both roughness coefficient values respectively, and for all prediction methods.

Table 4.9 Error analysis results for maximum individual overtopping volume prediction methods for CP placement method

Prediction method	**Predicted *q***	**MALE**	**RMSLE**
EurOtop (2018)	q_{calc} with γ_f = 0.50	1.2097	1.5633
	q_{calc} with $\gamma_{f,n}$=0.49	1.3015	1.6640
Molines et al. (2019)	q_{calc} with γ_f = 0.50	0.5225	0.6698
	q_{calc} with $\gamma_{f,n}$=0.49	0.5211	0.6774
Mares-Nasarre et al. (2020)	q_{calc} with γ_f = 0.50	0.4798	0.6340
	q_{calc} with $\gamma_{f,n}$=0.49	0.4727	0.6363

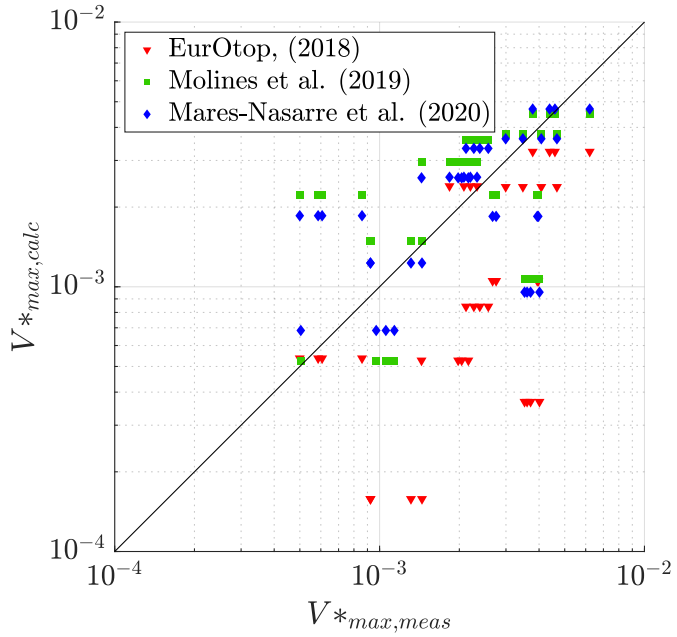

Figure 4.22 Comparison of measured and calculated maximum individual overtopping volumes for CP placement method (q_{calc} is predicted with γ_f = 0.50)

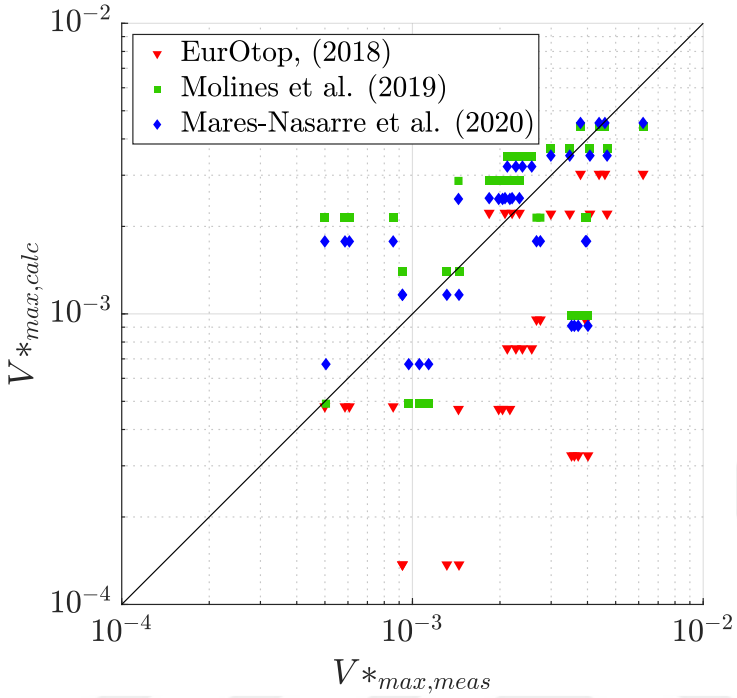

Figure 4.23 Comparison of measured and calculated maximum individual overtopping volumes for CP placement method (q_{calc} is predicted with $\gamma_{f,n}$)

For CP placement method, EurOtop (2018), again, heavily underestimates $V*_{max}$ predictions as it can be seen from Figure 4.22 and Figure 4.23, for γ_f and $\gamma_{f,n}$, thus yields large error results for both MALE and RMSLE (see Table 4.9).

Molines et al. (2019) and Mares-Nasarre et al. (2020) yield better and relatively close scatters in Figure 4.22 and Figure 4.23, however, there are still deviations from the measured values. According to the results given in Table 4.9, the error difference between Molines et al. (2019) and Mares-Nasarre et al. (2020) is 10% for MALE and 6% RMSLE less in favor of Mares-Nasarre et al. (2020).

For CP placement method, EurOtop (2018), it can be seen that using $\gamma_{f,n}$ for q_{mean} prediction increases the error for $V*_{max}$ prediction in contrast to two DP placement methods. Table 4.9Table 4.2 shows that MALE is increased by 8% and RMSLE is increased by about 7% when $\gamma_{f,n}$ is used instead of γ_f in maximum overtopping volume prediction.

For Molines et al. (2019), V^*_{max} prediction yields the same error results when $\gamma_{f,n}$ is used, for both MALE and RMSLE. Similarly, for Mares-Nasarre et al. (2020) MALE and RMSLE are almost the same when $\gamma_{f,n}$ is used in maximum overtopping volume prediction instead of γ_f (see Table 4.9).

In Figure 4.24 and Figure 4.25, $V^*_{max,meas}$ are compared with $V^*_{max,calc}$ by EurOtop (2018), Molines et al. (2019) and Mares-Nasarre et al. (2020) according to both γ_f (see Figure 4.24) and $\gamma_{f,n}$ (see Figure 4.25) for IR placement method. In Table 4.10, error analysis results of the data shown in Figure 4.24 and Figure 4.25, for both roughness coefficient values respectively, and for all prediction methods.

Table 4.10 Error analysis results for maximum individual overtopping volume prediction methods for IR placement method

Prediction method	**Predicted *q***	**MALE**	**RMSLE**
EurOtop (2018)	q_{calc} with γ_f = 0.50	1.1341	1.5155
	q_{calc} with $\gamma_{f,n}$=0.48	1.3285	1.7207
Molines et al. (2019)	q_{calc} with γ_f = 0.50	0.5509	0.6673
	q_{calc} with $\gamma_{f,n}$=0.48	0.5393	0.6547
Mares-Nasarre et al. (2020)	q_{calc} with γ_f = 0.50	0.4868	0.6135
	q_{calc} with $\gamma_{f,n}$=0.48	0.4560	0.6098

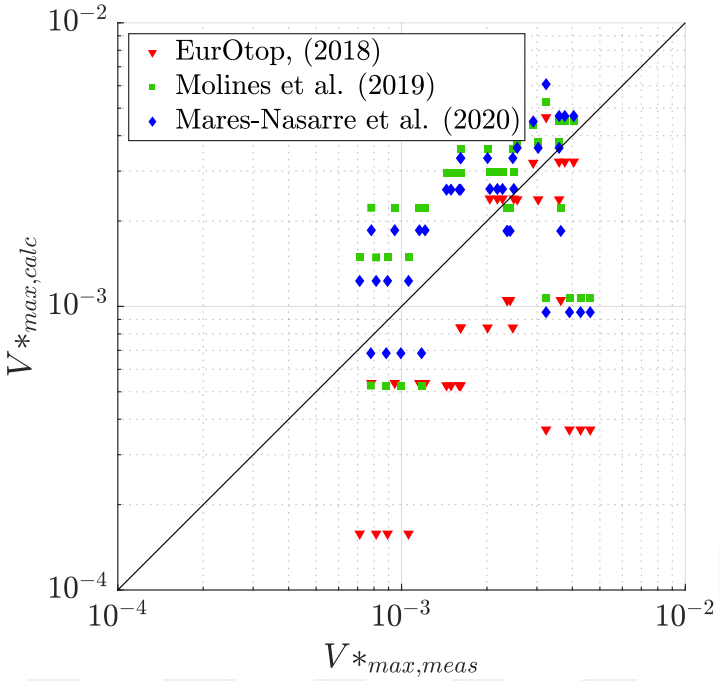

Figure 4.24 Comparison of measured and calculated maximum individual overtopping volumes for IR placement method (q_{calc} is predicted with $\gamma_f = 0.50$)

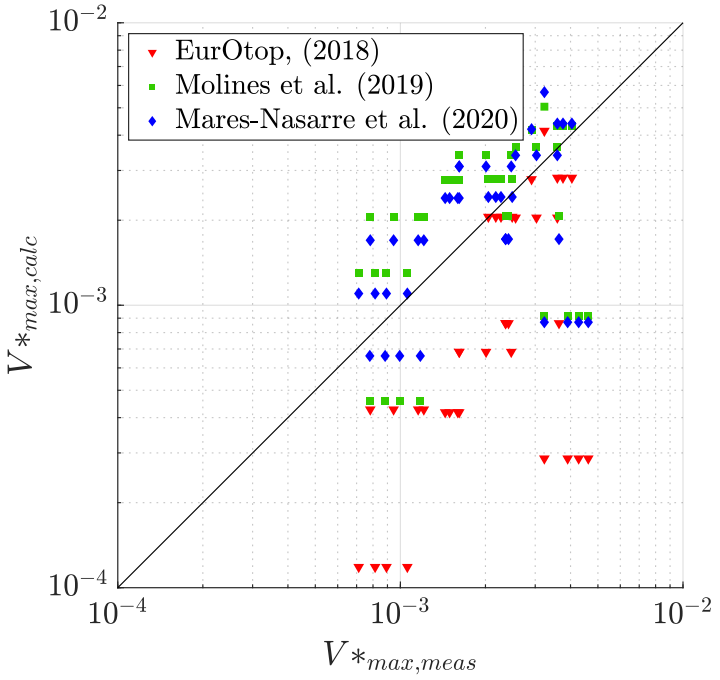

Figure 4.25 Comparison of measured and calculated maximum individual overtopping volumes for IR placement method

For IR placement method, EurOtop (2018), again, heavily underestimates V^*_{max} predictions as it can be seen from Figure 4.24 and Figure 4.25 for γ_f and $\gamma_{f,n}$ respectively, thus yields large error results for both MALE and RMSLE (see Table 4.10).

Molines et al. (2019) and Mares-Nasarre et al. (2020) yield better and relatively close scatters in Figure 4.24 and Figure 4.25. This scatter comparison is supported by error results in Table 4.10. The error difference between Molines et al. (2019) and Mares-Nasarre et al. (2020) is under 14% for MALE and 8% for RMSLE.

For IR placement method, EurOtop (2018), it can be seen that using $\gamma_{f,n}$ for q_{mean} prediction increases the error for V^*_{max} prediction similar to the CP placement method. Table 4.10Table 4.2 shows that MALE is increased by 15% and RMSLE is increased by about 13% when $\gamma_{f,n}$ is used instead of γ_f in maximum overtopping volume prediction.

For Molines et al. (2019), although error differences are small, also performs better when $\gamma_{f,n}$ is used, such that, MALE is reduced by 4% and RMSLE is reduced by 2%. Similarly, for Mares-Nasarre et al. (2020) MALE is reduced by 7% and RMSLE is reduced by 2% when $\gamma_{f,n}$ is used in maximum overtopping volume prediction instead of γ_f (see Table 4.8).

In Figure 4.26, Figure 4.27 and Figure 4.28, $V^*_{max,meas}$ are compared with $V^*_{max,calc}$ by EurOtop (2018), Molines et al. (2019) and Mares-Nasarre et al. (2020) for all placement methods. For Figure 4.26, $\gamma_f = 0.50$ is used for respective q_{calc} predictions. Similarly, in Figure 4.27, results of same procedure calculated with $\gamma_{f,n}$ are presented. Lastly, in Figure 4.28, instead of predicted mean overtopping discharges, measured values are implemented for all methods for comparison. In Table 4.11, error analysis results for all prediction methods and both roughness coefficient values.

Table 4.11 Error analysis results for maximum individual overtopping volume prediction methods

Prediction method	Predicted q	MALE	RMSLE
EurOtop (2018)	q_{calc} with $\gamma_f = 0.50$	1.3112	1.6950
	q_{calc} with $\gamma_{f,n}$	1.2433	1.6255
	q_{meas}	1.3505	1.5109
Molines et al. (2019)	q_{calc} with $\gamma_f = 0.50$	0.5115	0.6884
	q_{calc} with $\gamma_{f,n}$	0.4938	0.6362
	q_{meas}	0.3656	0.4787
Mares-Nasarre et al. (2020)	q_{calc} with $\gamma_f = 0.50$	0.4762	0.6438
	q_{calc} with $\gamma_{f,n}$	0.4599	0.6166
	q_{meas}	0.3655	0.4787

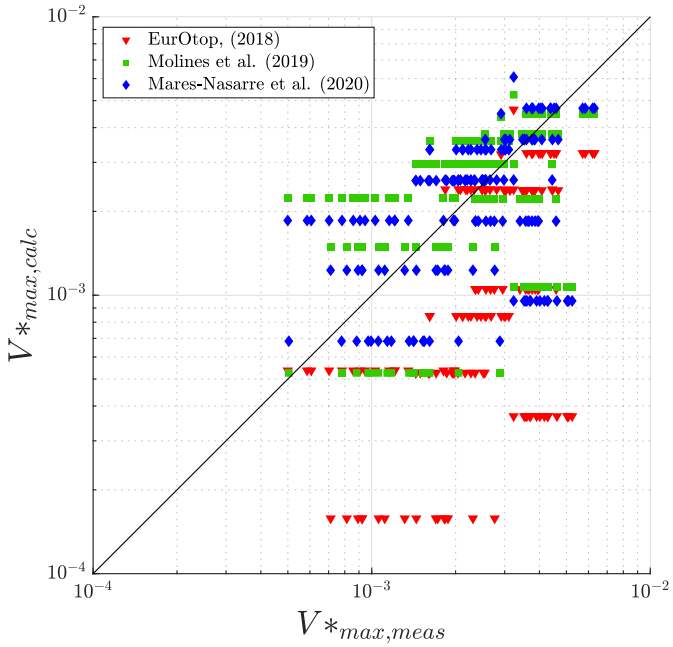

Figure 4.26 Comparison of measured and calculated maximum individual overtopping volumes where q_{calc} is predicted with $\gamma_f = 0.50$

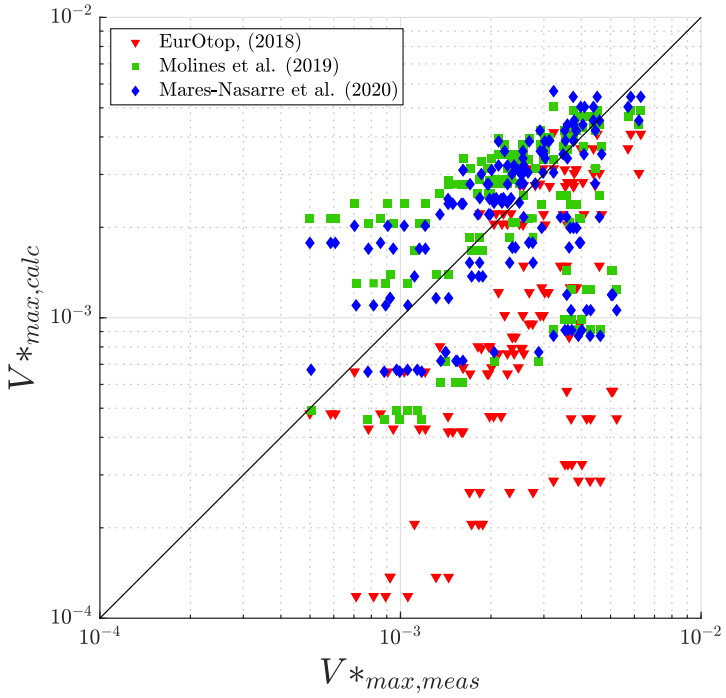

Figure 4.27 Comparison of measured and calculated maximum individual overtopping volumes where q_{calc} is predicted with $\gamma_{f,n}$

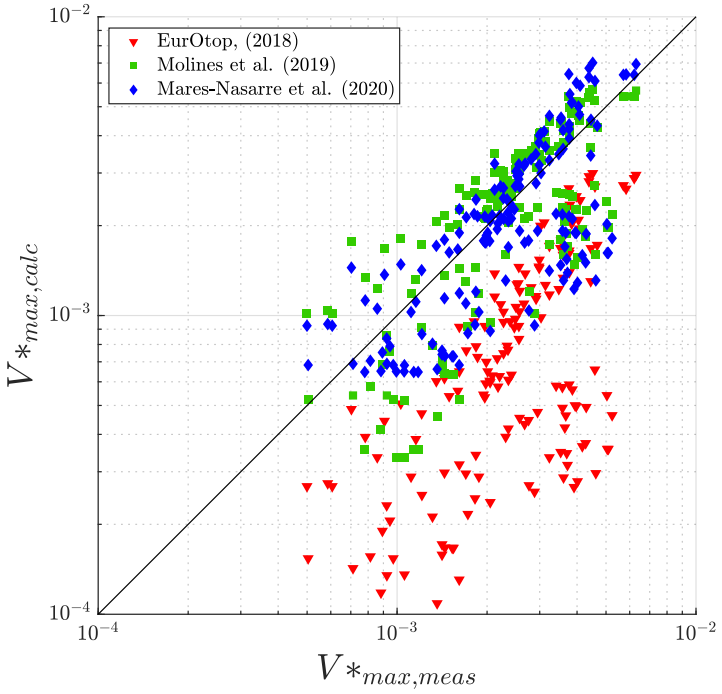

Figure 4.28 Comparison of measured and calculated maximum individual overtopping volumes where q_{meas} is used as prediction

For Figure 4.26, Figure 4.27 and Figure 4.28, Molines et al. (2019) and Mares-Nasarre et al. (2020) gives similar scatters with the former yielding slightly better results according to Table 4.11. While for Molines et al. (2019) MALE is reduced by 4% and RMSLE is reduced by 8%, for Mares-Nasarre et al. (2020) MALE and RMSLE are both reduced by 5% ,when $\gamma_{f,n}$ is used in maximum overtopping volume prediction (see Table 4.11). Lastly, using q_{meas} as the predicted value improves the results considerably, that shows as q_{mean} predictions gets closer to the measured values, V_{max} predictions becomes more and more accurate. As a result, when q_{meas} is used as the predicted mean overtopping discharge value, MALE is reduced by 27% and RMSLE is reduced by 26% for Molines et al. (2019) compared to predictions done based on $\gamma_{f,n}$ (see Table 4.11). Similarly, for Mares-Nasarre et al. (2020) MALE is reduced by 20% and RMSLE is reduced by 23% when q_{meas} is used in maximum overtopping volume prediction instead of q_{calc} is predicted with $\gamma_{f,n}$ (see Table 4.11).

On the other hand, EurOtop (2018) method notably has worse scatters and underestimates the predicted individual volumes for Figure 4.26, Figure 4.27 and Figure 4.28, that is also supported by error analysis results in Table 4.11. Although using q_{meas} as the predicted mean overtopping resuts improves the scatter similar to other two studies, Vmax values are still considerably underestimated, thus error results does not change much (see Table 4.11).

In conclusion, utilizing $\gamma_{f,n}$ improves V_{max} predictions as a result of more accurate q_{mean} predictions explained in Section 4.2.1. Molines et al. (2019) and Mares-Nasarre et al. (2020) gives similar results across all placement methods, which is expected since the latter uses the same framework of the first study. Moreover, Mares-Nasarre et al. (2020) states that the most accurate results for V_{max} predictions are obtained for Molines et al. (2019), however, their method is viable within their study's range ($0.33 \leq R_c/H_{m0} \leq 2.83$) that encompasses this study's range ($0.85 \leq R_c/H_{m0} \leq 1.78$), thus Mares-Nasarre et al. (2020) performed well for V_{max} predictions. Lastly, EurOtop (2018) performs worse than others in V_{max} predictions for all placement methods. All in all, the accuracy of maximum individual overtopping volume prediction mathods primarily depends on mean wave overtopping discharge prediction beside Weibull

distribuion parameters. As expected, CLASH NN performs better than a single formula for predicting mean wave overtopping discharges.

CHAPTER 5

CONCLUSION

The primary concern in designing rubble mound breakwaters, besides stability, is their serviceability, mainly determined by wave overtopping. Estimatipredictions.pping discharges is commonly done using empirical formulas available in the literature. The impact of different armor units on wave overtopping is considered by incorporating roughness coefficients (γ_f) into these formulas, which are widely accepted in design specifications. However, the influence of different placement methods for these units has not been fully explored or discussed.

To address this gap, a study was conducted to investigate the effect of various placement methods of antifer units on wave overtopping. The research involved experimental tests at the Coastal and Ocean Engineering Laboratory wave flume of Middle East Technical University's Department of Civil Engineering. A conventional rubble mound breakwater cross-section was constructed using antifer units with a 1:2 face slope and crown walls of varying crest heights (R_c). The study considered three antifer placement methods suggested in the literature: closed pyramid, double pyramid (regular and staggered), and irregular placement. Additionally, experiments were conducted with a total of eight different armor layers, each varying in packing densities, under different wave conditions with specific wave steepnesses and relative crest heights.

The findings of this study are outlined as follows:

- Based on the experimental findings, the study proposes new roughness coefficients ($\gamma_{f,n}$) for different antifer unit placement methods that improves mean wave overtopping discharge predictions for both prediction methods (EurOtop (2018) and CLASH NN) that have been investigated.

- The different placement methods and packing densities of antifer units significantly affect wave overtopping discharges. Specifically, the most significant difference observed was that the mean wave overtopping discharge rate is around 50% lower when antifer units are placed using the irregular placement method compared to the regular double pyramid method.
- Maximum individual overtopping volumes differ from mean wave overtopping discharges such that, maximum individual overtopping volumes are around 45% higher than mean overtopping discharges.
- The different placement methods of antifer units significantly affect maximum individual wave overtopping volumes. Specifically, the most significant difference observed was that the maximum individual wave overtopping volume rate is around 30% lower when antifer units are placed using the irregular placement method compared to the regular double pyramid method.
- For double pyramid placement method,it was observed that, staggering the upper layer by half nominal diameter of the antifer unit reduces the mean wave overtopping discharge by 20%.
- Three methods from the literature for maximum individual wave overtopping volume prediction on permeable rubble mound structures are evaluated. Since this prediction highly depends on mean wave overtopping prediction, the results supported the proposed new roughness coefficients.
- For two maximum overtopping volume prediction methods, Molines et al. (2019) and Mares-Nasarre et al. (2020) gives similar results across all placement methods, which is expected since the latter uses the same framework of the first study.
- Across all placement methods and roughness coefficent alternatives, CLASH NN provides a better estimation for mean wave overtopping discharge.

Nevertheless, there are still unresolved questions concerning the effects of armor layer unit placements on wave overtopping. These questions for future studies are listed as follows:

- The results of this study can be further improved by investigating a larger range wave conditions and relative crest elevations. A larger dataset for analysis shouldgive better estimations for roughness coefficient.
- Since there is a clear relationship between the armor unit placement methods and mean wave overtopping, other types of armor units should be investigated as well.
- Although the effect of packing density is clearer for double pyramid placement methods, its impact can be further researched for other placement methods with varying packing densities. This subject can also be extended for other armor unit types as well.
- A new formula can be derived for better maximum individual wave overtopping volume prediction based on the experimental and numerical analysis.

In summary, this research sheds light on the importance of considering the placement method and packing density of antifer units in the design of rubble mound breakwaters to better estimate wave overtopping discharges and enhance their serviceability.

REFERENCES

AYGM, (2016) “Kıyı Yapıları Planlama ve Tasarım Teknik Esasları”, T.C. Ulaştırma, Denizcilik ve Haberleşme Bakanlığı, Altyapı Yatırımları Genel Müdürlüğü.

Bruce, T., van der Meer, J. W., Franco, L., Pearson, J. M. (2009) “Overtopping performance of different armour units for rubble mound breakwaters”. Coastal Engineering, 56(2), 166–179.

Burcharth, H.F., Liu, Z., Troch, P. (1999) “Scaling of core material in rubble mound breakwater model tests”. Coastal and Port Structures, 1518–1528.

Eurotop (2018) “Eurotop 2018; Manual on wave overtopping of sea defences and related structures. An overtopping manual largely based on European research, but for worldwide application.”, Van der Meer, J.W., Allsop, N.W.H., Bruce, T., De Rouck, J., Kortenhaus, A., Pullen, T., Schüttrumpf, H., Troch, P. and Zanuttigh, B., www.overtopping-manual.com.

Franco, L., de Gerloni, M. and van der Meer, J.W. (1995) “Wave overtopping on vertical and composite breakwaters”, Coastal Engineering 1994 [Preprint].

Goda, Y. and Suzuki, T. (1976) “Estimation of incident and reflected waves in random wave experiments”, Coastal Engineering Proceedings, 1(15), p. 47.

Frens, A. B. (2007) “The impact of placement method on Antifer-block stability”. M.Sc. thesis, Delft University of Technology.

Klopman, G. and Meer, J.W. (1999) “Random wave measurements in front of reflective structures”, Journal of Waterway, Port, Coastal, and Ocean Engineering, 125(1), pp. 39–45.

Koosheh, A. et al. (2022) “Distribution of individual wave overtopping volumes at rubble mound seawalls”, Coastal Engineering, 177, p. 104173.

Mansard, E.P.D., Funke, E.R. (1980) “The Measurement of Incident and Reflected Spectra Using a Least Squares Method”, Hydraulics Laboratory Technical Report LTRHY-72, National Researc

Mares-Nasarre, P. et al. (2020) “Individual wave overtopping volumes on mound breakwaters in breaking wave conditions and gentle sea bottoms”, Coastal Engineering, 159, p. 103703.

Nørgaard, J.Q. et al. (2013) “Analysis of overtopping flow on sea dikes in oblique and short-crested waves”, Coastal Engineering, 76, pp. 43–54.

Nørgaard, J.Q. et al. (2013) “Analysis of overtopping flow on sea dikes in oblique and short-crested waves”, Coastal Engineering, 76, pp. 43–54.

Pan, Y. et al. (2016) “New understanding on the distribution of individual wave overtopping volumes over a levee under negative freeboard”, Journal of Coastal Research, 75(sp1), pp. 1207–1211.

Pedersen.J. (1996) “Wave Forces and Overtopping on Crown Walls of Rubble Mound Breakwaters”, Aalborg University, No. 12

Pillai, K., Etemad-Shahidi, A. and Lemckert, C. (2017) “Wave overtopping at Berm Breakwaters: Experimental Study and development of prediction formula”, Coastal Engineering, 130, pp. 85–102.

Schoonees, T., Kerpen, N.B. and Schlurmann, T. (2021) “Full-scale experimental study on wave overtopping at stepped Revetments”, Coastal Engineering, 167, p. 103887.

Soltanpour, M. and Yazdani, M. (2009) “Wave run-up at rubble mound breakwaters with antifer armor layers”, Coastal Structures 2007 [Preprint].

Van der Meer, J.W. (1988) “Rock slopes and gravel beaches under wave attack”. Ph.D. thesis, Delft University of Technology.

Van Gent, M. R. A. (1995) “Wave interaction with permeable coastal structures”. Communications on Hydraulic & Geotechnical Engineering - Delft University of Technology, 95–5(January 1995).

Victor, L. and Troch, P. (2010) ‘COASTLAB 2010’, in Proceedings on the Third International Conference on the Application of Physical Modelling to Port and Coastal Protection. Barcelona.

Yagci, O. and Kapdasli, S. (2003) “Alternative placement technique for antifer blocks used on Breakwaters”, Ocean Engineering, 30(11), pp. 1433–1451.

Yagci, O., Kapdasli, S. and Cigizoglu, H.K. (2004) “The stability of the antifer units used on breakwaters in case of irregular placement”, Ocean Engineering, 31(8–9), pp. 1111–1127.